Research Square

Preprints are preliminary reports that have not undergone peer review.
They should not be considered conclusive, used to inform clinical practice,
or referenced by the media as validated information.

Techno-Economic Feasibility of Green Hydrogen and Oxygen Production at Pilot and Industrial Scales Using Photovoltaic-Powered Solid Oxide Electrolysis in Barrancabermeja, Colombia

Giovanni Morales-Medina

gmorales@uis.edu.co

Universidad Industrial de Santander

Research Article

Keywords: Energy integration, Electrolysis, SOEC, Photovoltaic system, Simulation, LCOH

Posted Date: November 17th, 2026

DOI: https://doi.org/10.21203/rs.3.rs-10659000/v1

License: This work is licensed under a Creative Commons Attribution 4.0 International License.
Read Full License

Additional Declarations: No competing interests reported.

Techno-Economic Feasibility of Green Hydrogen and Oxygen Production at Pilot and Industrial Scales Using Photovoltaic-Powered Solid Oxide Electrolysis in Barrancabermeja, Colombia

Giovanni Morales-Medina

Universidad Industrial de Santander, Escuela de Ingeniería Química, Cra. 27 Calle 9, Bucaramanga, Colombia, A.A.680002

Correspondence: gmorales@uis.edu.co

https://orcid.org/0009-0006-5215-0512

Abstract

The integration of photovoltaic energy with solid oxide electrolysis cells (SOEC) offers a promising route for large-scale green hydrogen production in regions with high solar potential. This study presents the first techno-economic assessment in Colombia to explicitly incorporate oxygen co-product valorization into photovoltaic-driven hydrogen production systems. An integrated framework combining Aspen HYSYS simulation, photovoltaic system sizing, and financial analysis was applied to evaluate pilot- (0.02 t/day H_2) and industrial-scale (46.6 t/day H_2) SOEC systems in Barrancabermeja. The proposed configurations achieved H_2 and O_2 purities of 99.8 vol% and 99.6 vol%, respectively, at 800 °C and pressures up to 30 bar, with a specific electrical energy consumption of ~32 kWh/kg H_2. While the pilot-scale operation was not economically viable, the industrial-scale system deployment achieved positive NPV, high IRR, and levelized costs of $9.65 USD/kg H_2 and $2.40 USD/kg O_2. The results highlight the importance of scale, oxygen valorization, and integrated system design for economically viable green hydrogen production.

Keywords: Energy integration; Electrolysis; SOEC; Photovoltaic system; Simulation; LCOH.

Statements and Declarations

Competing Interest

The author declare no competing financial interest or personal relationship that could have influenced the work reported in this paper.

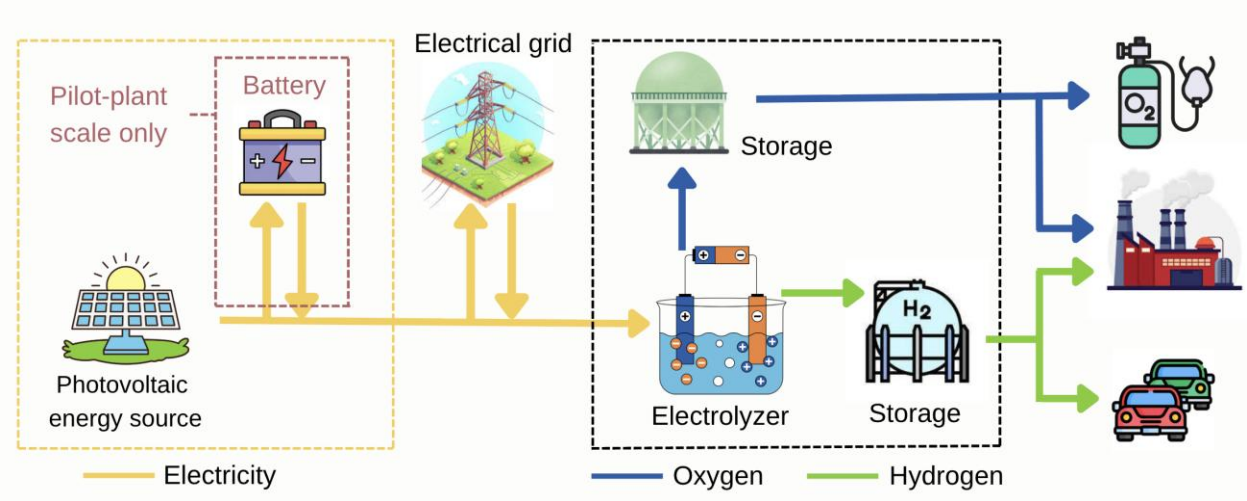
Generative AI and AI-assisted technologies in the manuscript preparation process

During the preparation of this work, the authors used ChatGPT (OpenAI) to assist with English language editing and improve manuscript clarity. Following its use, the authors carefully reviewed and revised the content as needed and take full responsibility for the final version of the manuscript. All scientific content, analyses, and conclusions were developed solely by the author, and the tool was used exclusively for language refinement purposes.

Funding

This research received no external funding.

Graphical abstract



Highlights:

- The first Colombian techno-economic assessment incorporating O_2 valorization in green H_2 systems is presented.
- Industrial-scale deployment (46.6 t/day H_2) achieved positive NPV, high IRR, and LCOH of $9.65 USD/kg H_2.
- Balance-of-plant equipment and storage systems dominated total CAPEX in large-scale SOEC deployment.
- Legal incentives reduce $LCOH$ from 13.18 to 9.65 USD/kg at the industrial scale.
- An economic-potential-based PV sizing methodology was proposed for integrated H_2–O_2 production systems.

1. Introduction

The reduction of environmental impacts and the enhancement of energy security are key priorities in international agendas and energy-transition strategies worldwide (Sun et al. 2021; IEA 2023). Among the main strategies for achieving these goals are the expanded deployment of renewable energy sources and the development of low-carbon fuels. In this context, green hydrogen (H_2) is produced through water electrolysis powered by renewable sources such as photovoltaic (PV) and wind energy. Since most countries have access to water and renewable resources, H_2 production contributes to energy security, environmental sustainability, and energy equity by serving as a versatile energy carrier (Abe et al. 2019). Water electrolysis also generates oxygen (O_2) at approximately eight times the mass of H_2 produced, making it an important co-product that may contribute significantly to the economic viability of hydrogen projects (Eckl et al. 2024). Different roadmaps highlight hydrogen production and its application in transportation, industry, residential buildings, and power generation (Sadiq et al. 2023; Agbadaola et al. 2024). For example, South Korea's roadmap aims to supply 5% of national energy consumption with hydrogen by 2040, reducing greenhouse gas emissions by approximately 27 Mt (Stangarone 2021). Similarly, Japan's roadmap (Council 2019) and the Netherlands' greenhouse gas reduction program (FCH 2019a) target 0.3 Mt of H_2 production and 3–4 GW of hydrogen-derived energy capacity by 2030, respectively. The European Hydrogen Roadmap also envisions blending H_2 with natural gas for applications such as iron reduction furnaces by 2030 (COM 2020; FCH 2019b). Meanwhile, the U.S. Department of Energy has established a target levelized cost of hydrogen ($LCOH$) of $1.0 USD/kg by the 2030s (US Department of Energy 2020). Likewise, Colombia's Hydrogen Roadmap aims to reduce the $LCOH$ to $1.7 USD/kg by the 2030s, through the installation of 1–3 GW of electrolysis capacity, with particular emphasis on the Caribbean region (Minenergía 2021). However, these roadmaps generally do not explicitly address strategies for O_2 purification, storage, and valorization.

The main challenges associated with achieving H_2 production and $LCOH$ targets are the capital expenditures ($CAPEX$) of PV system (Henbest et al. 2021; IEA 2019a) and the operating expenditures ($OPEX$) of the electrolysis technologies (Sadiq et al. 2023; Kumar and Himabindu, 2019). Several studies indicate that these costs are expected to decrease over the coming decades due to economies of scale and technological advances, although the magnitude of the reduction strongly depends on the energy context of each country (Sadiq et al. 2023; Henbest et al. 2021; IEA 2019b; Kumar and Himabindu, 2019; Zainal et al. 2024; Martsinchyk et al. 2024). These reductions are expected to accelerate the large-scale deployment of green hydrogen technologies. Reported $LCOH$ values for photovoltaic-driven

electrolysis systems typically range between $2–9 USD/kg depending on electricity price, climatic conditions, electrolyser technology, and system integration strategy. Bukar et al. (2024) reported that in Thailand, commercial electricity prices strongly influence the design of PV-based hydrogen production systems, with estimated $LCOH$ values of $3.7–6.5 USD/kg for electricity costs ranging from $0.02–0.22 USD/kWh. Abomazid et al. (2022) studied PV-H_2 cost minimization in Ontario, Canada, considering local climatic conditions, and reported an $LCOH$ of $5–9.4 USD/kg. Similarly, Zghaibeh et al. (2022) analyzed the economic viability of a 300 kg/day PV-H_2 plant and estimated an $LCOH$ of $6.7 USD/kg. Shehabi and Dally (2021) projected H_2 production in Kuwait using PEM and SOEC electrolysers and electricity costs of $0.021–0.0478 USD/kWh, obtaining an $LCOH$ of $2.09–4.41 USD/kg. Jang et al. (2022) compared $LCOH$ values across different electrolysers and found that SOEC systems achieved the lowest costs. Collectively, these studies demonstrate that electricity price, electrolyser technology, and renewable resource availability remain the dominant factors governing green H_2 economics.

To support hydrogen production targets, several countries promote H_2 development through fiscal policies and incentives. In Colombia, Law 1715 of 2014 (Ley-1715) regulates incentives for electricity generation from non-conventional renewable sources (CONPES-3934 2018), while Law 2099 of 2021 (Ley-2099) expanded this framework to include H_2. Additionally, CONPES 3934 promotes energy diversification through renewable integration (CONPES-3934 2018). The impact of fiscal incentives has been analyzed in multiple studies (García-García et al. 2023; Ropero-Castaño et al. 2022; Guzman and Henao 2022; Arias-Gaviria et al. 2019; Perez and Garcia-Rendon 2020; Sallyth and Ramos 2021; López et al. 2020; Muñoz et al. 2024; Manuel et al. 2023; Betancur et al. 2023), highlighting their critical role in project viability. Currently, Colombia produces approximately 8.8 t/year of H_2 from pilot PV plants operated by public and private companies (Semana 2022a; Ecopetrol 2022; Promigas 2022; Semana 2022b). Recent reports also indicate that 26 projects are in the planning or installation phase, which may contribute to the expansion of H_2 deployment and utilization in the coming years (Fenoge 2023; Portafolio 2024). Nevertheless, limited disclosure of technical and financial information, including O_2 co-product valorization, introduces uncertainty regarding progress toward roadmap targets. The growing interest in green H_2 has also motivated several techno-economic and environmental studies focused on the Colombian context. Velasquez-Jaramillo et al. (2024) analyzed alkaline and PEM systems integrated with renewable sources in Uribia, La Guajira, reporting an $LCOH$ of $8.4 USD/kg for an average production of 6.8 t/h while incorporating fiscal incentives into the financial assessment. However, their cash flow projections lacked detailed $CAPEX$ breakdowns for balance-of-plant (BOP) equipment, as

well as depreciation considerations. Burdack et al. (2023) projected $LCOH$ trends for the 2030–2050 period, based on $CAPEX$ and $OPEX$ estimates from IEA's World Energy Outlook 2021. Their study focused on PV-based H_2 generation in La Guajira and reported an $LCOH$ values between \$3.24–1.65 USD/kg for 2030–2050 period. Rodríguez-Fontalvo et al. (2023) estimated a national production potential of 8.2 Mt H_2 by 2050 with an electricity demand of 212 GW under a "Solar Intensive" scenario, although without providing detailed financial data. Moreno et al. (2022) and Plazas-Niño et al. (2023) focused primarily on environmental impacts. Erazo-Cifuentes et al. (2022) evaluated H_2 supply chain configurations in the Colombian Caribbean region, using simplified formulations for $LCOE$ and $LCOH$ estimation. Their results suggested that, by 2030, the optimal configuration would combine wind-based H_2 production with storage and gas compression systems for transport. Additional studies have also projected $LCOE$ and $LCOH$ values but frequently rely on simplified assumptions for equipment sizing, system performance, and cost estimation, without incorporating broader financial indicators (Erazo-Cifuentes et al. 2022; Rincón-Montenegro et al. 2024; Benalcazar and Komorowska 2024; Ríos et al. 2024; Nadaleti et al. 2022; Fontalvo et al. 2023). Despite these contributions, most studies on green H_2 production in Colombia remain focused on planning-level analyses and macro-scale projections. Consequently, detailed engineering-based conceptual design, integrated techno-economic analysis, and explicit consideration of O_2 purification, storage, and valorization remain largely unexplored in the Colombian context. Considering Colombia's favorable solar resources and industrial infrastructure, these aspects are essential for accurately evaluating the feasibility of large-scale green H_2 deployment. Colombia's geographical conditions are favorable for PV-based H_2 production. Barrancabermeja exhibits an average solar irradiation of 4.0–5.5 kWh/m^2/day (IDEAM 2015), exceeding global averages (Figure 1). As the location of the country's largest refinery (ECOPETROL-GRB), it offers significant infrastructure advantages for H_2 integration. To address the identified gaps, this work presents a techno-economic feasibility assessment of H_2 and O_2 co-production using a PV-powered solid oxide electrolysis cell (SOEC) system in Barrancabermeja. High-temperature electrolysis was selected due to its higher efficiency and favorable operating conditions (US Department of Energy 2020; Henbest et al. 2021; IEA 2019a; Motazedi et al. 2021; Posdziech et al. 2019), with a current technology readiness level (TRL) of 6–7 (IEA 2019b; Jang et al. 2022; InsightAce Analytic Pvt. 2023).

The proposed methodology consists of three phases. Phase I involves process simulation in Aspen HYSYS v14 to estimate yields and generate the data required for the design and technical feasibility assessment of the H_2 production system. The process is defining at two scales: a pilot-scale plant, producing 0.02 t/day of H_2 using a PV

system with battery storage, and an industrial-scale plant, producing 46.6 t/day of H_2 using a PV system with grid connection. The pilot-scale configuration is consistent with the facility installed at the Refinery of Cartagena (RefiCar) in Colombia (Semana 2022a; Ecopetrol 2022), whereas the industrial-scale configuration is comparable to the production capacity of a steam methane reforming (SMR) unit at ECOPETROL-GRB (Martínez-González et al. 2024). Phase II focuses on sizing the PV system for each scale, based on solar irradiation data from Barrancabermeja and the total energy requirements of each configuration. Phase III comprises the financial evaluation and sensitivity analysis of H_2 production at both scales, including $CAPEX$, $OPEX$, and a 20-year cash flow analysis incorporating Colombian legal incentives.

2. Models and Methods

2.1 Process Simulation. Hydrogen production through a solid oxide electrolysis cell (SOEC) was simulated in Aspen HYSYS v14 and the Peng–Robinson equation of state. This thermodynamic package was selected due to its demonstrated capability to represent high-temperature gaseous mixtures containing H_2, O_2, and H_2O, as well as its widespread application in hydrogen process simulations (Sladkovskiy et al. 2018; Zhang et al. 2022). The process flow diagram is presented in Figure 2 for the industrial-scale configuration and in Figure S1 for the pilot-scale configuration. The SOEC was modeled as a conversion reactor coupled with a component separator representing the cathode and anode compartments (Motazedi et al. 2021; JaeHwa et al. 2010). In the proposed process, the feed water stream (H2O_feed) was mixed with recycled hydrogen (H2_recycle) before entering the SOEC, where electrolysis occured at 800 °C and 1.4 bar, producing H_2, O_2, and unreacted H_2O. The inlet composition was defined as 90 mol% H_2O and 10 mol% H_2 (Motazedi et al. 2021; JaeHwa et al. 2010; McKellar et al. 2007; O'Brien et al. 2005). The hydrogen fraction was included to maintain reducing conditions at the cathode and improve electrochemical stability during operation. A steam conversion of 88.9% was assumed based on reported values for high-temperature electrolysis systems (McKellar et al. 2007), while a pressure drop of 3% across the electrolyser was considered (Ranjbar et al. 2014; Sadeghi et al. 2015). The SOEC outlet stream was subsequently separated into a cathode stream (H2–H2O h) and an anode stream (O2_anode).

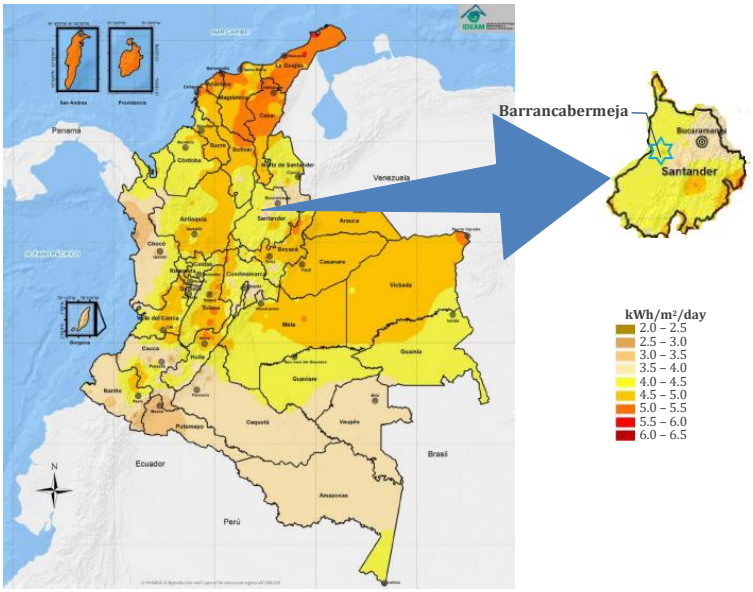
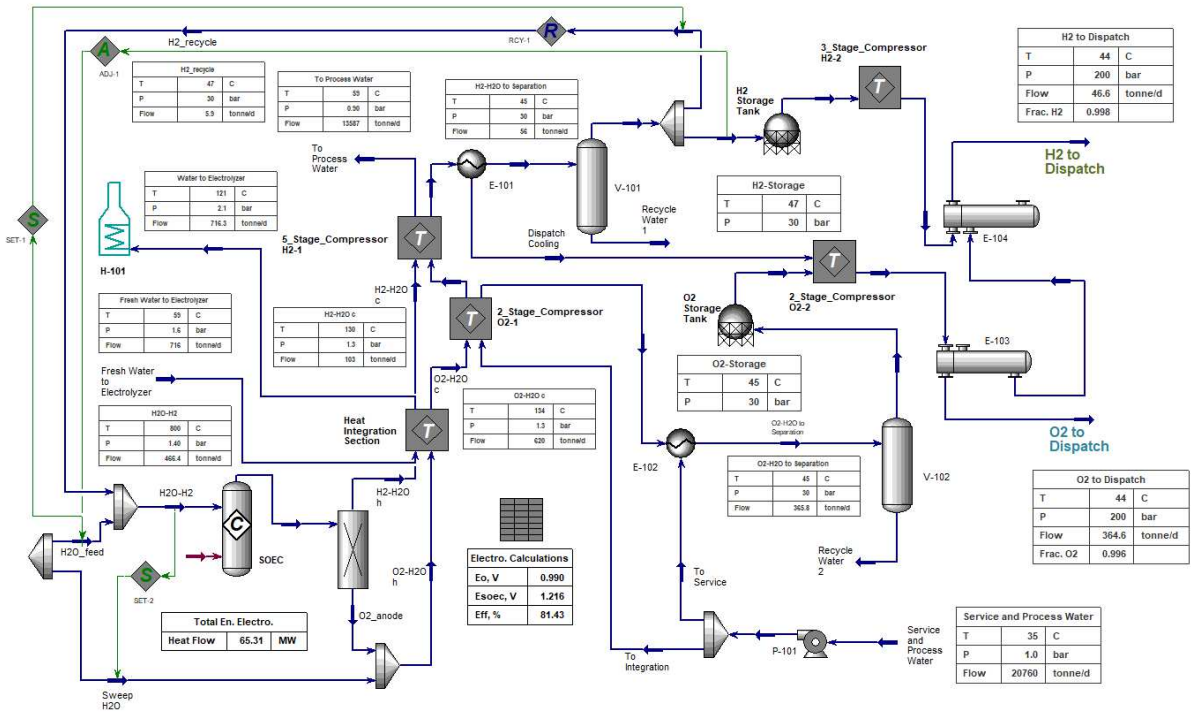


Fig. 1 Average annual solar irradiation (kWh/m^2/day) in Colombia and Barrancabermeja (IDEAM 2015).

The cathode outlet stream was cooled from 800 °C to 130 °C within a heat integration section prior to compression and downstream purification. A five-stage compression train increased the pression to 30 bar, consistent with operation conditions commonly reported for above-ground H_2 storage systems (Zoulias and Lymberopoulos 2007; Kalinci et al. 2015; Gutiérrez-Martín et al. 2020; Khan et al. 2021a). Subsequent cooling and phase separation enabled water recovering and the H_2 purification to 99.8 vol%. Approximately 88.9% of the purified hydrogen was directed to storage, whereas the remaining fraction was recycled to the SOEC inlet to maintain reducing cathode conditions and improve electrochemical stability (Zhao et al. 2021). The stored H_2 was further compressed to 200 bar for transportation through steel tube trailers (Khan et al. 2021b; Reddi et al. 2018; Vives et al. 2023). The anode outlet stream was mixed with steam (Sweep H2O) to promote O_2 entrainment and enhance oxygen recovery. The stream was subsequently cooled and compressed to 30 bar followed by condensation and phase separation to obtain O_2 with a purity of 99.6 vol%, corresponding to industrial-grade oxygen (Ministerio de la Protección Social, 2009; ICONTEC 2008). The purified O_2 was stored and later compressed to 200 bar for transportation. Detailed sub-flowsheets for the compression and purification systems are provided in Figures 3a–e and Figure S2 for the pilot-scale configuration.

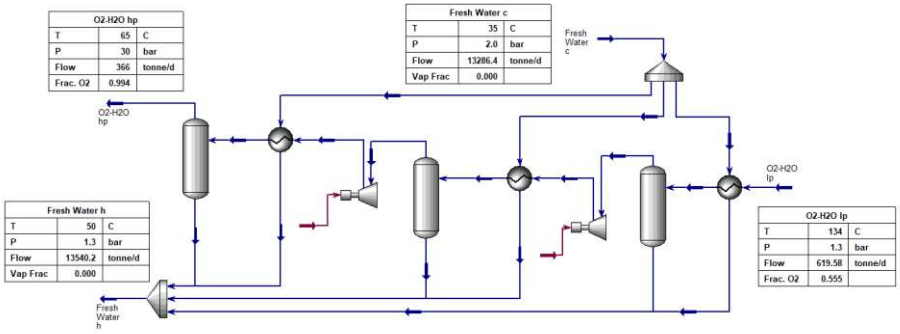


187

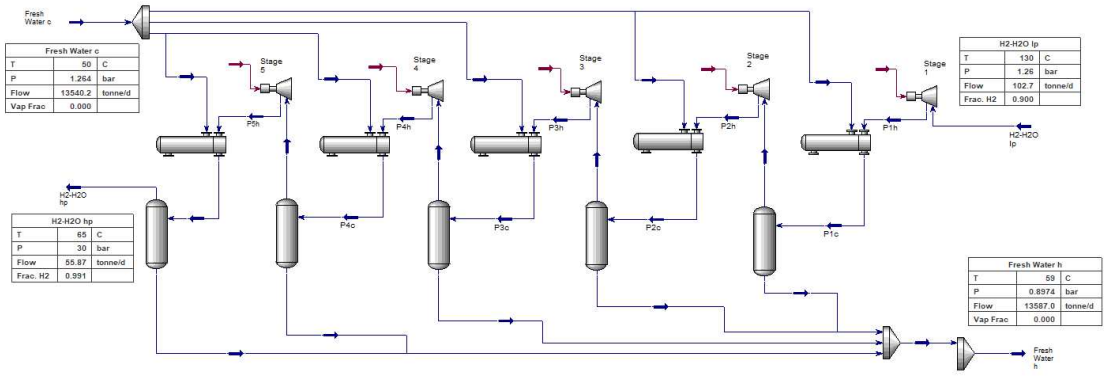
188 **Fig. 2** Process flow diagram (PFD) of H_2 and O_2 generation at industrial scale simulated in Aspen HYSYS v14.

189 Thermal integration was incorporated to reduce auxiliary heating demand and improve overall system
190 efficiency. Process water was used as cooling medium in the hydrogen and oxygen compression systems and in the
191 heat integration section. The recovered thermal energy was subsequently used to preheat the electrolyser feed stream
192 prior to final heating in furnace H-101. The proposed thermal integration strategy reduced external vaporization energy
193 requirements by approximately 48%, thereby improving thermal efficiency and reducing auxiliary utility
194 consumption. The total inlet water flowrates corresponded to 7.99 ton/day at pilot scale and 20,760 ton/day at
195 industrial scale. After heat recovery and cooling duties, the outlet water streams left the system at approximately 54
196 °C and may be reused for steam generation or auxiliary thermal services. All heat exchangers were sized using Aspen
197 EDR (Aspen Exchanger Design & Rating). The main simulation assumptions are summarized in Table 1. Simulation
198 convergence was achieved using the Set, Recycle, and Adjust objects available in Aspen HYSYS. The Set objects
199 were employed to define the recirculated hydrogen flow and entrainment steam requirements, whereas the RCY-1
200 object controlled the recycle convergence loop. The ADJ-1 object regulated the hydrogen production flowrate to
201 satisfy the target operating conditions. The simulation framework was validated through comparison of specific
202 electrical energy consumption, operating voltage, hydrogen purity, and thermoneutral operating conditions against

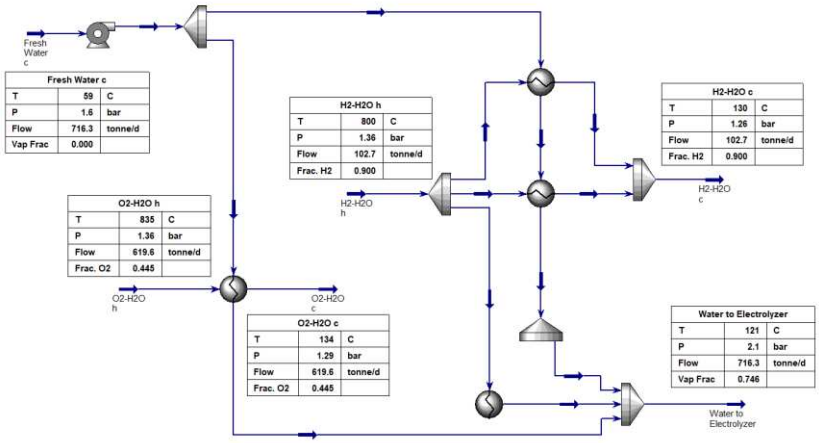
values reported in previous SOEC studies (Motazedi et al. 2021; JaeHwa et al. 2010; O'Hayre et al. 2009; Abad et al. 2021).



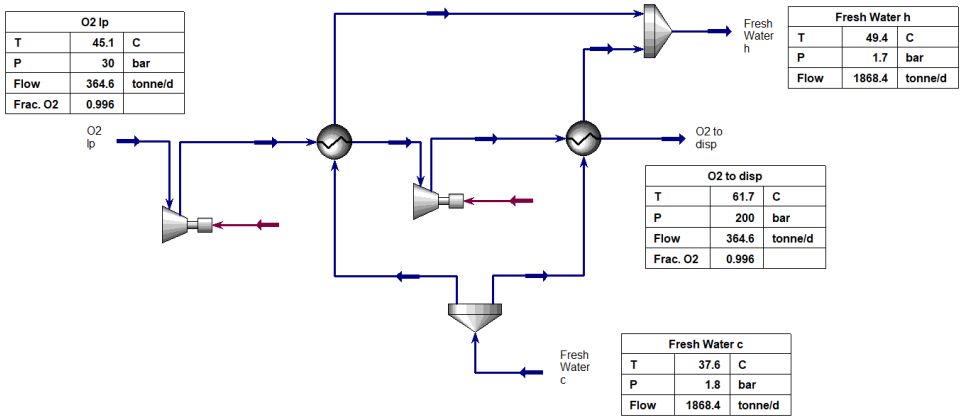
(a) 2_Stage_Compressor O2-1



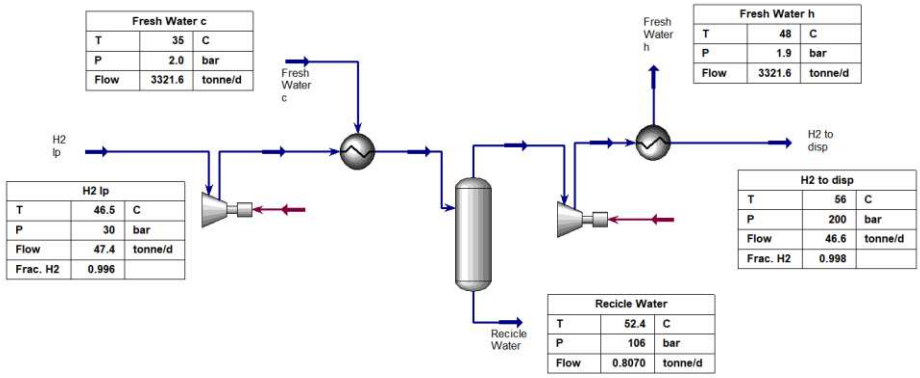
(b) 5_Stage_Compressor H2-1



(c) Heat Integration Section



(d) 2_Stage_Compressor O2-2



(e) 3_Stage_Compressor H2-2

Fig. 3 Sub-flowsheet objects defined for the H_2 and O_2 generation simulated in Aspen HYSYS v14 with results for the industrial scale.

Table 1. Assumptions for the simulation.

Electrolyser
Inlet mass flow ratio: H_2O/H_2 = 9 (Motazedi et al. 2021; JaeHwa et al. 2010; McKellar et al. 2007; O'Brien et al. 2005)
Operation conditions: 1.4 bar, 800 °C (Motazedi et al. 2021; JaeHwa et al. 2010; McKellar et al. 2007; O'Brien et al. 2005)
Conversion: 88.9% (McKellar et al. 2007)
Pressure drop: 3% (Ranjbar et al. 2014; Sadeghi et al. 2015)
Sweep steam: half of molar inlet flow to electrolyser (Motazedi et al. 2021; JaeHwa et al. 2010; McKellar et al. 2007; O'Brien et al. 2005).
Balance-Of-Plant Section (BOP)
H_2 production: Pilot plant 20 kg/day and Industrial scale 46.6 t/day

Compressors: efficiency 80% (Masters 2013)
Compression ratio (CR) for H_2: CR = 2 (Reddi et al. 2018; Utgikar and Thiesen 2006)
Compression ratio (CR) for O_2: CR = 4 Schmidt et al. 2017)
Minimum approach temperature for heat exchangers: 8 °C (McKellar et al. 2007; O'Brien et al. 2005)
Pressure for storage tanks: 30 bar (Zoulias and Lymberopoulos 2007; Kalinci et al. 2015; Gutiérrez-Martín et al. 2020; Khan et al. 2021a)
Pressure for dispatching: 200 bar (Khan et al. 2021b; Vives et al. 2023; Ministerio de la Protección Social, 2009; ICONTEC 2008; León-Vargas et al. 2018; Wang et al. 2019)
Heat exchangers pressure drop each side: calculated by Aspen EDR (default 3 kPa).

The electrical power required for electrolysis (W_{SOEC}) was calculated from the applied cell voltage (E_{SOEC}), current density (i), and total electrode area (A), according to Eq. (1). The applied voltage was determined from the Nernst potential (E_{Nernst}), operating temperature (T), pressure (P), and area-specific resistance (ASR), as expressed in Eqs. (2-4) (JaeHwa et al. 2010; O'Brien et al. 2005; Utgikar and Thiesen 2006; O'Hayre et al. 2009).

$$W_{SOEC} = E_{SOEC} * i * A \quad (1)$$

$$E_{SOEC} = E_{Nernst} + i * ASR \quad (2)$$

$$E_{Nernst} = 1.253 - \frac{2.4516T}{10^4} - \frac{RT}{2F} ln\left(\frac{P_{H2O}}{P_{H_2} P_{O2}^{0.5}}\right) \quad (3)$$

$$ASR = -0.213 + 3.973 * 10^{-5} e^{10,300/T} \quad (4)$$

In Eq. (3), R and F represent the ideal gas constant and the Faraday constant (96,485 C/mol), respectively. This formulation enables estimation of SOEC electrical requirements under varying operating conditions while maintaining computational efficiency within the process simulation framework. The current density (i) was selected to achieve thermoneutral operation, corresponding to an applied voltage close to 1.29 V at 800 °C (O'Hayre et al. 2009; Abad et al. 2021; Hauck et al. 2017). Commercial SOEC systems are typically composed of stacks with active areas up to 550 cm^2, limited by thermal stress and gas distribution considerations, enabling hydrogen production capacity close to 22 kg/h per stack (Hauck et al. 2020; Lahrichi et al. 2024; Gniewomir and Ghassan 2023; Tomberg 2024). Based on these limitations, one module was considered sufficient for pilot-scale production, whereas twelve modules with nominal hydrogen production capacity of 4 t/day each were required for industrial-scale operation. Cells were connected in series to form stacks, while stacks were arranged in parallel to form modules (Sakas et al. 2022; Ghezel-Ayagh 2023). The total electrode area (A) was calculated using Eq. (5) (Motazedi et al. 2021):

$$A = \frac{2F}{i} \dot{H} \quad (5)$$

where $\dot{H}$ represents the hydrogen molar production rate. The calculated electrode area was subsequently distributed across stacks and modules to determine the total number of cells required. Eqs. (1–5) were implemented in Aspen HYSYS using the Spreadsheet object. The effects of current density, recycle fraction, inlet temperature, and operating pressure were evaluated using the Case Studies tool. The analyzed parameter ranges were: current density from 0.2 to 1.0 A/cm^2, recycle fraction from 0.01 to 0.4, inlet temperature from 600 to 1000 °C, and pressure from 1 to 30 bar. In total, 18,900 fully converged simulations were performed considering both production scales. The optimal operating conditions were identified through parametric minimization of a cost-based objective function derived from the simulation outputs. The optimization variables included current density, recycle fraction, operating temperature, and pressure, while hydrogen production rate was maintained fixed for each production scale. The objective function incorporated $CAPEX$ contributions associated with the PV system, electrolyser modules, and land requirements, together with the discounted five-year $OPEX$ contributions related to heating, cooling, pumping, and maintenance. A reduced-five-year operational horizon was adopted during optimization to emphasize the short-term economic sensitivity of process operating conditions during conceptual design. Long-term degradation and stack replacement costs were excluded from the optimization stage due to uncertainties associated with SOEC degradation mechanisms under industrial operation. The optimization was conducted through exhaustive parametric evaluation of 18,900 fully converged simulation cases. The objective function is expressed in Eq. (6):

$$Cost\ Function = CAPEX_{PV} + CAPEX_{Elect} + CAPEX_{Land} + OPEX^{0}_{h/c} + OPEX^{0}_{pump} + OPEX^{0}_{maint} \quad (6)$$

Dynamic degradation effects, transient renewable fluctuations, and long-term electrochemical aging mechanisms were not explicitly modeled and should be considered in future studies. Nevertheless, the proposed optimization framework enables identification of operating conditions that minimize both investment and operational expenditures during the conceptual design stage of photovoltaic-driven SOEC systems.

2.2 Design of the Photovoltaic System. The PV system was sized to satisfy the electrical energy demand of the SOEC process. The number of PV panels ($\boldsymbol{n}$) was calculated using Eq. (7), adapted from Mulcué-Nieto (2020), considering minimum panel efficiency under local climatic conditions, as well the optimal azimuth and tilt angles for Barrancabermeja. In Eq. (7), $\boldsymbol{P_m}$ represents the nominal panel power (kW) under standard test conditions, $\boldsymbol{W}$ is the annual electrical energy demand (kWh/year), and $\boldsymbol{HSP}$ corresponds to the equivalent peak sun hours.

$$n = \frac{W}{193.45 * P_m * HSP} \quad (7)$$

The annual electrical demand ($\boldsymbol{W}$) was estimated from the SOEC, BOP and storage power requirements obtained through process simulation. The HSP represent the number of daily hours with an irradiance equivalent to 1 kW/m^2 and were determined from the area under the monthly average irradiance curve. Figure 4 presents the average daily solar irradiance in Barrancabermeja, obtained from the System Advisor Model (SAM) developed by NREL (Blair et al. 2018). The calculated HSP values (Figure 5) range from 3.69 to 6.29 h, with a minimum in August, a maximum in April, and an annual average of 4.75 h per day, consistent with reported values for Colombian cities (León-Vargas et al. 2019). The influence of HSP on economic performance was evaluated through $LCOE$ and an economic potential function (EP), defined in Eq. (8). The formulation incorporates revenues associated with surplus electricity export ($Rev^0_{Surplus}$, Eq. 9), PV investments ($CAPEX_{PV}$), land costs ($CAPEX_{Land}$), maintenance costs ($OPEX^0_{maint}$), and electricity purchase costs during irradiation deficit periods ($OPEX^0_{lack}$, Eq. 10).

$$EP\ (HSP) = Rev^0_{Surplus} - CAPEX_{PV} - CAPEX_{Land} - OPEX^0_{maint} - OPEX^0_{lack} \quad (8)$$

$$Rev^0_{Surplus} = Price^0_{selling} * Power_{total} * \sum_{HSP_i>HSP} \left(\frac{HSP_i}{HSP} - 1\right) \quad (9)$$

$$OPEX^0_{lack} = Cost^0_{pur} * Power_{total} * \sum_{HSP_i<HSP} \left(1 - \frac{HSP_i}{HSP}\right) \quad (10)$$

The HSP value that maximizes the EP function was selected for PV system sizing. Battery storage was included only for the pilot-scale configuration due to its autonomous operating strategy and relatively low power demand. The number of batteries was estimated assuming 14 h of operation without solar irradiation. In contrast, battery storage was excluded for the industrial-scale configuration due to the large investment and land requirements associated with high-capacity storage systems. The number of batteries was used to calculate using Eq. (11) (McCormick et al. 2016; Masters 2013):

$$Bat = \frac{t*W}{Cap*V} \quad (11)$$

where t is the required operating time (h), W is the electrical power demand (W), Cap is the battery capacity (Ah), and V is the battery voltage (V).

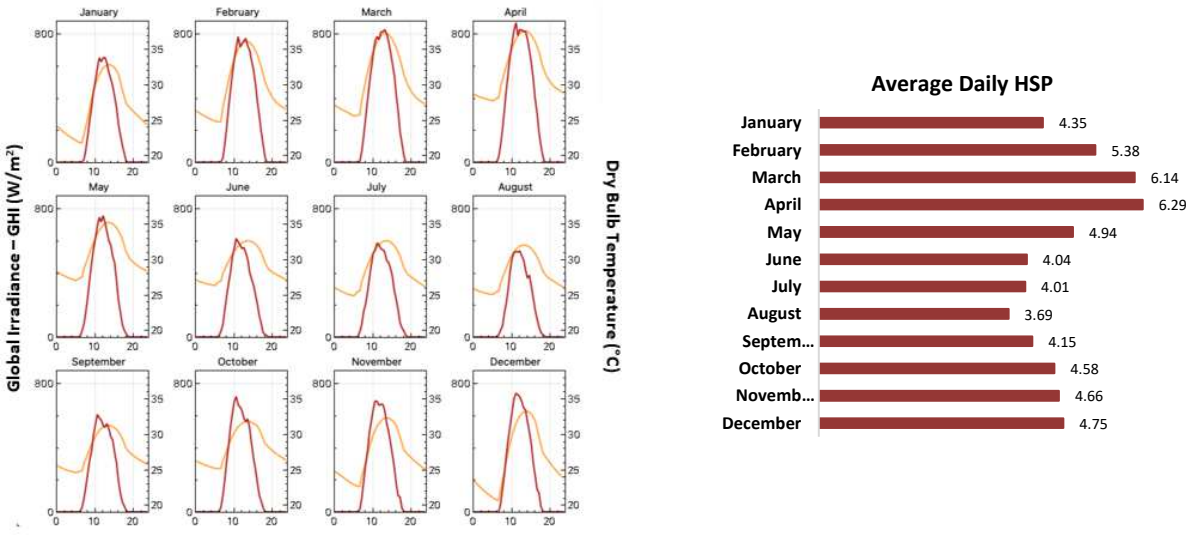


Fig. 4 Monthly average daily variation of solar radiation (red), temperature (yellow), and hours of solar peak (HSP) in Barrancabermeja (Blair et al. 2018).

2.3 Capital and Operational Expenditure. The $CAPEX$ includes direct plant costs (installation, instrumentation and control, piping, electrical facilities, buildings, yard improvements, and service facilities), indirect plant costs (engineering, supervision, and construction expenses), contractor's fee, legal expenses, contingency, and working capital. Table 2 summarizes the characteristics and costs of the PV system components. Equipment specifications and base costs were obtained from AutoSolar Inc. Installation costs for the PV system and electrolyser-related equipment were estimated as 15% of PV equipment cost and 12% of electrolyser equipment costs, respectively, following previous techno-economic studies (Hinkley et al. 2016). Land cost **(**$CAPEX_{Land}$) was calculated assuming $17,500 USD/ha based on the total PV installation area.

Table 2. Description and cost of photovoltaic system components.

Component	Description	Cost
Panel	Deep-Blue MBB JAM66S30 500W – 38V – 13 A, Efficiency: 21% 132 cells (2.1 m x 1.13 m x 30 mm) Weight: 26.3 kg NOCT = 45 °C. Lifespan: 25 years	$0.3 USD/W
Battery	Tensite GEL 12-250 Lifespan: 5 years Normal capacity: 250 Ah Weight: 57.0 kg	$367.1 USD/bat
Converters (DC-DC, AC-DC)	Efficiency: 95% Lifespan: 10 years	$773.3 USD/converter
Charge controller	MUST PC1500B PWM Nominal current: 50 A, 12V	$45.0 USD/controller

Lifespan: 10 years

Reported free-on-board (FOB) costs for SOEC systems range between 2,000 and 4,000 €/kW depending on plant capacity and manufacturing scale (Kumar and Himabindu, 2019; Lähdemäki 2021; Wang et al. 2019; Schmidt et al. 2017; Vidas and Castro 2021). Accordingly, specific costs of 4,000 €/kW and 2,000 €/kW were assumed for pilot- and industrial-scale configurations, respectively, reflecting expected economies of scale (Bui et al. 2023; Harboe et al. 2020). The process additionally requires heat exchangers for thermal integration, steam condensation, compressor intercooling, and product conditioning. Heat exchanger costs (USD) were estimated using Eqs. (12–15) (Seider et al. 2017), based on the heat transfer area obtained from Aspen HYSYS simulations:

$$C_{Fl-head} = (2.7 + 0.7244A^{0.07})F_p \exp(12.031 - 0.8709\,ln(A) + 0.09005\ln^2(A)) \quad (12)$$

$$C_{Fx-head} = (2.7 + 0.7244A^{0.07})F_p \exp(11.4185 - 0.9228\,ln(A) + 0.09861\ln^2(A)) \quad (13)$$

$$F_p = 0.9803 + 1.8 * 10^{-4}P + 1.7 * 10^{-7}P^2 \quad (14)$$

$$C_{FH} = 1.7F_p exp(-0.15241 + 0.785\,ln(Q)) \quad (15)$$

Where A is the heat transfer area (ft^2), P is the operating pressure (psig), and Q corresponds to the heat duty (BTU/h). Eq. (12) and Eq. (13) (Seider et al. 2017) were applied for estimating cooler costs in pilot- and industrial-scale configurations, respectively, whereas Eq. (15) was used for fire heater estimation. Flash drums were incorporated for phase separation of H_2O from H_2- and O_2-rich streams. Vessel costs were estimated using Eqs. (16–20) (Seider et al. 2017):

$$C_p = C_V + C_{PL} \quad (16)$$

$$W = \pi(D + t)(L + 0.8D)t\rho \quad (17)$$

$$C_V = exp[10.5449 - 0.4672\ln(W) + 0.05482(\ln(W))^2] \quad (18)$$

$$C_{PL} = 410D^{0.7396}L^{0.70684} \quad (19)$$

Where C_V represents the cost of the vessel shell (USD), C_{PL} corresponds to platforms and ladder costs (USD), D is the internal diameter (in), t is the vessel wall thickness (in), and L is the vessel height (in), and ρ is the steel density (0.284 lb/in^3). The wall thickness was determined according to ASME pressure vessel criteria (Eq. 20) (Peters et al. 2002):

$$t = Pr_i(0.8S - 0.2P)^{-1} + C_A \quad (20)$$

Where r_i is the internal radius (in), S is the allowable stress (15,000 psi), and C_A is the corrosion allowance (0.12 in). Hydrogen storage capacity was defined as one day of production, corresponding to 8.6 m^3 for pilot scale and 20,060.3 m^3 for industrial scale under storage conditions of 30 bar. Metallic storage systems become progressively more expensive at high pressures due to increased wall thickness requirements (Paneru et al. 2024). Therefore, composite-based storage technologies were considered, using reported costs ranging from \$270 to \$673.9 USD/kg H_2 (Houchins et al. 2022; Barthelemy et al. 2017; Maggio et al. 2022; Klymyshyn et al. 2023). Costs of \$673.9 USD/kg H_2 and \$270 USD/kg H_2 were assumed for pilot- and industrial-scale systems, respectively, reflecting scale-dependent reductions in storage costs. Oxygen storage was estimated using analogous cost assumptions.

The number of compressor stages was determined from recommended compression ratios (CR). For oxygen compression, a single-stage compression ratio of 4 was adopted (Walas 1988), whereas for hydrogen a ratio of 2 was selected to limit discharge temperatures and facilitate intercooling (Khan et al. 2021a-b; Reddi et al. 2018; Seider et al. 2017). The required number of stages was calculated using Eq. (21):

$$n_c = \frac{\log\left(\frac{P_d}{P_s}\right)}{\log(CR)} \tag{21}$$

Where, P_s and P_d represent suction and discharge pressures, respectively. Compressors costs were estimated from the break horsepower (BHP), obtained from Aspen HYSYS, using Eq. (22):

$$C_{PC} = 1.15 * 2.5exp[9.1553 + 0.63\ln(BHP)] \tag{22}$$

All equipment costs were updated to 2026 values using the Chemical Engineering Plant Cost Index ($CEPCI$), according to Eq. 24, assuming a $CEPCI$ correction factor of 1.58 (ChemEng 2026):

$$FOB_{2026} = FOB_{2017}\left(\frac{CEPCI_{2026}}{CEPCI_{2017}}\right) \tag{23}$$

The total $CAPEX$ was estimated using the Lang factor methodology (Seider et al. 2017; Peters et al. 2002), which incorporates direct and indirect costs, contractor fees, legal expenses, contingencies, and working capital:

$$CAPEX = 1.05 f_L \sum FOB_{2026_i} \tag{24}$$

where f_L=5.93 corresponds to fluid process plant (Peters et al. 2002). The Lang-factor approach was selected because the study corresponds to a conceptual feasibility assessment, where detailed engineering information remains unavailable and factorial estimation methods are widely accepted for early-stage techno-economic analyses.

2.4 Future Cash Flows and Financial Indicators. A discounted cash flow analysis was developed for both production scales considering a project lifetime of 20 years. Annual operating time was assumed as 8,200 h/year to account for scheduled shutdowns and operational interruptions (Lähdemäki 2021; Wang et al. 2019). Operation and maintenance (O&M) costs were estimated as 2% of total CAPEX. Base-case selling prices were assumed as \$10 USD/kg H_2 and \$5 USD/kg O_2 considering industrial and medical-grade oxygen markets (Maggio et al. 2022; Giorgianni et al. 2025). Utility costs were defined as follows (Garcia-Vallejo and Alzate 2024; Garcia-Vallejo and Alzate 2024b): \$6.08 USD/GJ for steam, \$0.07 USD/kGal for water, \$0.079 USD/kWh for natural gas, and \$0.06 USD/kWh for electricity. Direct wages and benefits ($DW\&B$) were estimated using Eq. (25) (Seider et al. 2017):

$$DW\&B = 5N * H_{op} * Salary \quad (25)$$

where N is the number of operators per shift (2 for pilot scale, 12 for industrial scale), H_{op} is the annual operation time (2,184 h), and $Salary$ is the hourly wage (\$20 USD/h). Replacement costs were considered for batteries (every 5 years), inverters and controllers (every 10 years), and the SOEC modules. Based on reported SOEC lifetime of 60,000–90,000 h (Schmidt et al. 2017), two electrolyser replacements were considered during the project lifetime. Replacement costs of €1,300/kW and €700/kW were assumed for the first and second SOEC replacements, respectively (Schmidt et al. 2017; Harboe et al. 2020). Future PV replacement costs were adjusted assuming a 50% reduction in PV system costs by 2050 (Mauler et al. 2021; IRENA 2019). Cash flows were calculated in USD, considering an annual inflation rate of 2.53% (NREL 2023). EBITDA (earning before interest, taxes, depreciation and amortization) was estimated as the difference between revenues and $OPEX$ (Lähdemäki 2021), while net cash flow included amortization, depreciation, taxes, and fiscal incentives. Fiscal incentives were incorporated according to Colombian Law 1715 of 2014 and associated regulations, including: VAT and import tariff exemptions, accelerated depreciation (33.33% per year), and income tax reductions for renewable energy investments. Financial performance was evaluated through net present value (NPV), internal rate of return (IRR), profitability index (PI), $LCOE$, $LCOH$, and $LCOO$, according to Eqs. (26-31) (Velasquez-Jaramillo et al. 2024; Vartiainen et al. 2021; Aldersey-Williams and Rubert 2019; Awad et al. 2024):

$$NPV = \sum_{t=0}^{20} \frac{F_t}{(1+i)^t} \quad (26)$$

$$0 = \sum_{t=0}^{20} \frac{F_t}{(1+IRR)^t} \quad (27)$$

$$PI = \frac{1}{CAPEX} \sum_{t=1}^{20} \frac{F_t}{(1+i)^t} \quad (28)$$

$$LCOE = \frac{CAPEX_{PV}^0 + OPEX_{PV}^0}{Y_{PV}^0} \quad (29)$$

$$LCOH = \frac{CAPEX_{Tot-H2}^0 + OPEX_{Tot-H2}^0}{M_{H2}^0} \quad (30)$$

$$LCOO = \frac{CAPEX_{Tot-O2}^0 + OPEX_{Tot-O2}^0}{M_{O2}^0} \quad (31)$$

The nominal weighted average annual cost of capital ($WACC_{nom}$) was assumed as 7.0% (NREL 2023; CREG 2021), while a real $WACC$ of 5.5% (Jiménez-Martín et al. 2024) was used for IRR comparison. Projects were considered viable when $IRR > WACC_{real}$. The payback period was defined as the time required for cumulative discounted cash flow to reach zero.

2.5 Financial sensitivity analysis. A one-at-a-time sensitivity analysis was conducted to evaluate the influence of key economic parameters on $LCOH$ and $LCOO$. The analyzed variables included $CAPEX$, $OPEX$, H_2 and O_2 selling prices, and the nominal weighted average cost of capital ($WACC_{nom}$). Each parameter was independently varied within a range of ±30% relative to the base-case scenario. For each variation, $LCOH$ and $LCOO$ were recalculated, while maintaining all remaining parameters constant. This methodology enables direct identification of the dominant economic drivers affecting systema profitability and levelized production costs. The sensitivity analysis was performed independently for pilot- and industrial-scale configurations in order to evaluate the effect of production scale on economic robustness. The proposed framework additionally provides insight into the resilience of the hydrogen production system under uncertain market, financing, and policy conditions.

3. Results and Discussion

3.1 Simulations of SOEC and Balance-of-Plant Systems. Table 3 summarizes the main simulation results obtained for both production scales. At pilot scale, the system produces 0.02 t/day of H_2 (99.8 vol%) and 0.155 t/day of O_2 (99.6 vol%) using 0.177 t/day of fresh water and 0.003 t/day of recycled H_2. At industrial scale, the production increases to 46.6 t/day of H_2 (99.8 vol%) and 364.6 t/day of O_2 (99.6 vol%), requiring 460.5 t/day of fresh water and 5.9 t/day of recycled H_2. The electrical and thermal demand increase substantially with production scale. The pilot-scale configuration requires 0.026 MW of electrical power and 0.002 MW of thermal power, whereas the industrial-scale system demands 61.95 MW and 3.36 MW, respectively. Additional heating the H_2 recycle stream to 800 °C requires approximately 0.5 kWh at pilot scale and 2.11 MWh at industrial scale. The estimated specific energy consumption is 31.91 kWh/kg H_2 (electrical) and 1.73 kWh/kg H_2 (thermal), remaining within the range reported for high-temperature electrolysis systems (Motazedi et al. 2021; JaeHwa et al. 2010; Ni et al. 2007). Under operating conditions of 800 °C and 1.4 bar, the calculated Faraday efficiency reaches 81.43% (Ferrero et al. 2023; Hu et al. 2022), reflecting electrical losses associated with activation, ohmic, and concentration overpotentials, during charge transport. Thermoneutral operation is achieved at a current density of approximately 0.39 A/cm², corresponding to electrode areas of 5.53 m² for pilot scale and 13,070 m² for industrial scale. These requirements translate into one stack (101 cells) for pilot scale and 98 stacks (237,637 cells) for industrial operation, each operating at approximately 215 A (Hauck et al. 2020; Lahrichi et al. 2024; Gniewomir and Ghassan 2023).

Table 3. Simulation results for the SOEC system at pilot and industrial scales.

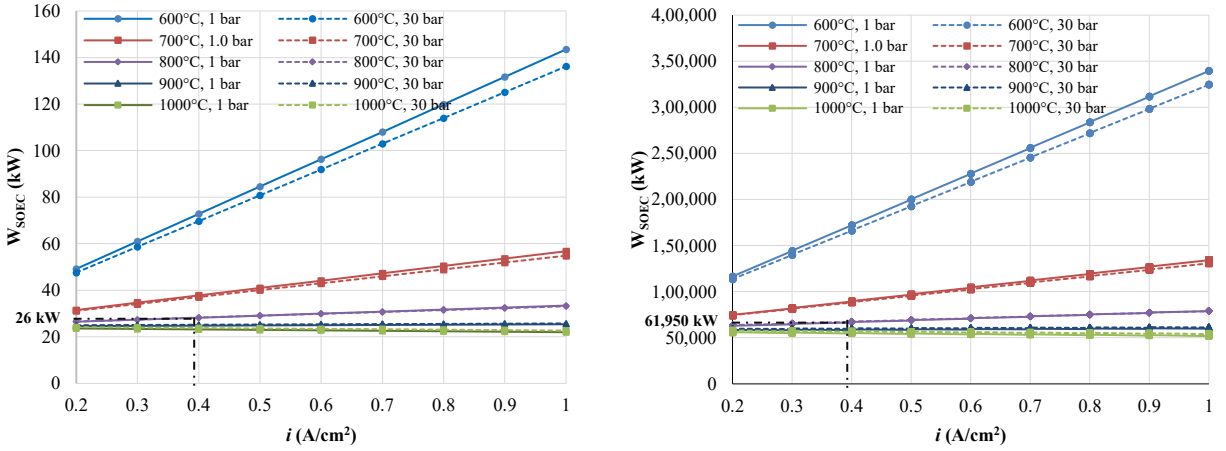
Parameter	Pilot Scale	Industrial Scale
Fresh water to electrolysis	0.195 t/day (858 °C, 1.4 bar)	460.5 t/day (858 °C, 1.4 bar)
Fresh water to sweep	0.108 t/day (858 °C, 1.4 bar)	255.8 t/day (858 °C, 1.4 bar)
Total fresh water to process	7.991 t/day	20760 t/day
Recycle stream	0.003 t/day of H_2 (47 °C, 30 bar)	5.9 t/day of H_2 (47 °C, 30 bar)
Electrode area (m²)	5.53	13,070
Number of stacks	1	98*
Cells (550 cm² per cell)	101	237,637
Stack voltage (kV)	0.131	307
Stack current (A)	215	215
Electrical power, W_{SOEC} (MW)	0.026	61.95
Thermal power, Q_{SOEC} (MW)	0.003	3.36
Electrical heating of feed water (MW)	0.008	----

Parameter	Pilot Scale	Industrial Scale
Thermal heating of feed water (MW)	----	17.77
Compression (MW)	0.004	9.78
Pumping (MW)	$1.2*10^{-5}$	0.033
Baterry charge (MW)	0.058	
Total electricity requirement (MW)	0.097	75.12
Hydrogen production	0.02 t/day (99.8 vol%)	46.6 t/day (99.8 vol%)
Oxygen production	0.155 t/day (99.6 vol%)	364.6 t/day (99.6 vol%)

Note: Operational conditions in the electrolyser, E_{Cell} =1.28 V, current density i=0.40 A/cm^2, 800 °C, 1.4 bar. *Stacks arranged in four modules.

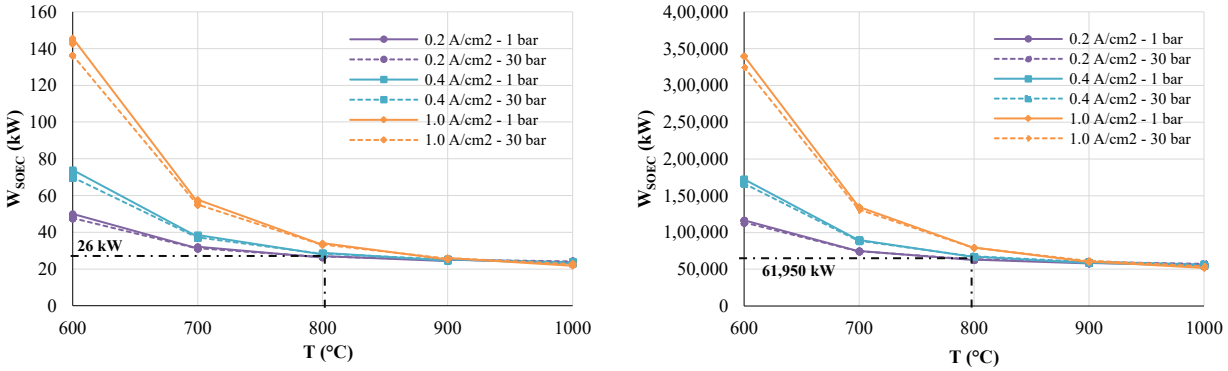
Figures 5–6 present the parametric analysis performed using the Aspen HYSYS Case Studies tool, with the selected operating point indicated by the red dashed line. Figures 5a–b show the variation of electrolyser electrical power consumption (W_{SOEC}) as a function of current density (i) at different temperatures (T) and pressures (P = 1 and 30 bar). As expected, W_{SOEC} increases approximately linearly with current density, at constant T, due to the direct increase in electrochemical reaction rate and associated irreversible losses. Increasing pressure slightly decreases power demand because pressurized operation improves gas diffusion and reduces polarization effects. Figures 6a–b show that increasing T, at fixed i, significantly reduces W_{SOEC}, particularly between 600 °C and 700 °C, where electrochemical kinetics and ionic conductivity improve substantially. Above 800 °C, the influence of current density becomes less pronounced, and the power demand stabilizes at approximately 22–24 kW for pilot scale and 52–54 MW for industrial scale, depending on pressure and operating current density. These results confirm the strong thermodynamic advantage of high-temperature electrolysis (Motazedi et al. 2021; JaeHwa et al. 2010; Ni et al. 2007; Wang et al. 2021). The effect of pressure on electrolyser efficiency is presented in Figures S3a–b. Increasing pressure slightly reduces efficiency up to ~10 bar, after which the effects become negligible (Ferrero et al. 2023; Gaikwad et al. 2023). At 30 bar, 800 °C, and 0.40 A/cm², efficiency is only ~5% lower than under atmospheric conditions. Although pressurized operation improves hydrogen and oxygen diffusion through electrodes, it may accelerate stack degradation and reduce long-term durability (Tomberg 2024; Beyrami et al. 2026). Temperature exerts a substantially larger influence than pressure. Electrolyser efficiency decreases markedly below 800 °C due to higher activation and ohmic losses (Wang et al. 2021; Beyrami et al. 2026; Cheng et al. 2021; Laguna-Bercero et al. 2023), whereas efficiency gains above this temperature become progressively limited, with only an additional improvement of approximately 8% between 800 °C and 1000 °C. Similar trends are observed for specific energy consumption (Figures

S4a–b), which decreases sharply with temperature, particularly between 600 and 700 °C, where reductions of approximately 46.8% are obtained. Conversely, increasing current density increases specific energy consumption almost linearly by approximately 2 kWh/kg H_2 for every 0.2 A/cm² increase in current density. Therefore, operation at relatively low current densities and elevated temperatures are advantages from operating-cost perspective.



(a) Pilot Scale (b) Industrial Scale

Fig. 5 Variation of electric potential as a function of current density in high-temperature electrolysis.

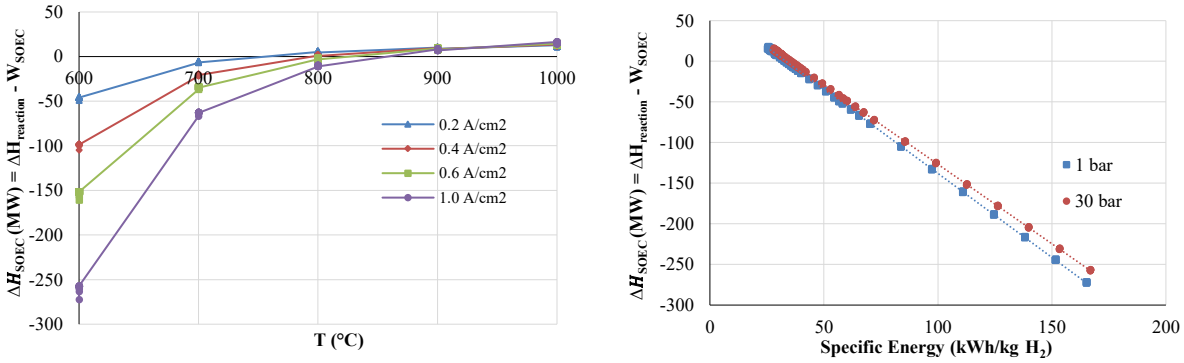


(a) Pilot Scale (b) Industrial Scale

Fig. 6 Variation of electric potential as a function of temperature in high-temperature electrolysis.

Thermoneutral operation constitutes one of the most critical operation conditions for efficient SOEC performance. Figures 7a–b present the variation of ΔH_{SOEC} ($\Delta H_{reaction} - W_{SOEC}$) as a function of temperature and specific energy consumption. Thermoneutral conditions ($\Delta H_{SOEC} = 0$) occur within approximately 750–850 °C for current densities between 0.2 and 0.6 A/cm², consistent with previous studies (Motazedi et al. 2021; JaeHwa et al.

2010; O'Hayre et al. 2009; Abad et al. 2021; Hauck et al. 2017; Wang et al. 2021). Specifically, thermoneutral operation is achieved at approximately 0.2 A/cm² at 750 °C, 0.4 A/cm² at 800 °C, and 0.6 A/cm² at 850 °C. Operation below the thermoneutral temperature leads to negative ΔH_{SOEC} values, corresponding to exothermic behavior dominated by irreversible electrochemical losses. Under these conditions, excess heat generation requires external cooling and reduces overall efficiency (Beyrami et al. 2026; Laguna-Bercero et al. 2023). Conversely, operation above thermoneutrality results in endothermic behavior, where external heat input partially offset electrical demand, thereby reducing W_{SOEC}. However, excessively high temperatures increase thermal management requirements and accelerate stack degradation mechanisms such as sintering, delamination, and microstructural instability (Beyrami et al. 2026; (Yan and Li 2025; Giridhar et al. 2024). Consequently, the optimal operating window lies within 750–850 °C, where the balance between electrical efficiency, thermal demand, and stack durability becomes most favorable. Figure 7b additionally shows that thermoneutral conditions correspond to minimum specific energy consumption, approximately 34 kWh/kg H_2 at 1 bar and 38 kWh/kg H_2 at 30 bar.

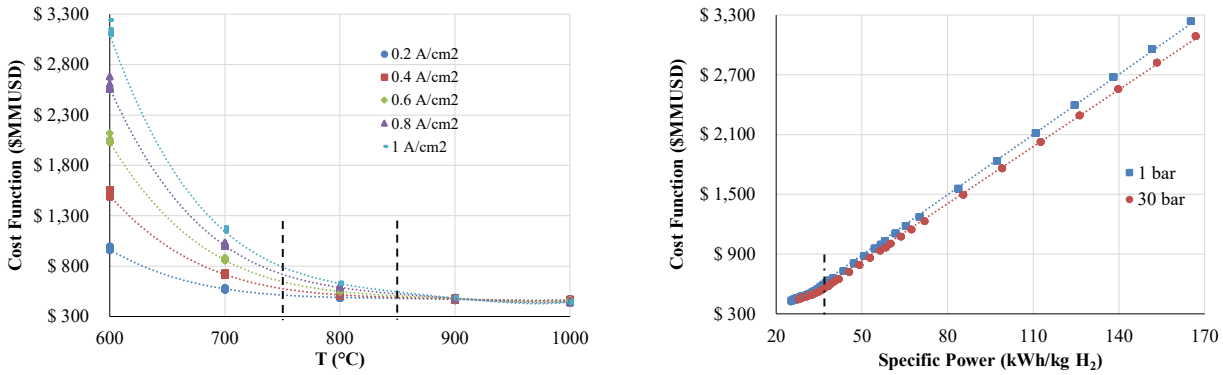


(a) Temperature (b) Specific energy consumption

Fig. 7 Variation of the difference between the heat of reaction ($\Delta H_{reaction}$) and the electrical work (W_{SOEC}) for high-temperature electrolysis at the industrial-scale system as a function of (a) temperature and (b) specific energy consumption.

Figures S5a–b illustrate the inverse relationship between electrode area (A) and current density (i). At pilot scale, the required A decreases from 10.9–11.8 m² at 0.2 A/cm² to 2.2–2.4 m² at 1.0 A/cm², while at industrial scale, A decreases from 26,000–27,700 m² to 5,200–5,500 m² over the same range. Increasing current density from 0.2 to 1.0 A/cm² reduces A by approximately 80%, confirming that i is the dominant design variable controlling electrolyser size. Nevertheless, increasing current density does not necessarily reduce overall $CAPEX$ because SOEC costs are

generally expressed per installed electrical capacity rather than per unit electrode area (Lähdemäki 2021; Wang et al. 2019; Schmidt et al. 2017). Moreover, higher current densities substantially increase electrical consumption and may accelerate stack degradation due to thermal stresses, sintering, and microstructural changes (Gniewomir and Ghassan 2023; Yan and Li 2025; Giridhar et al. 2024). The effect of pressure on A is comparatively small with only approximately 7% reduction when pressure increases from 1 to 30 bar, indicating limited economic benefit from pressurization. Excessive reductions in A may additionally limit H_2 transport through the porous electrode structure, adversely affecting efficiency and production stability (Trinke and Bensmann 2017). Therefore, the selection of current density requires balancing electrode area, electrical efficiency, degradation rate, and operational cost. Based on these considerations, a Pareto-optimal operating point was selected. Figures S5a–b indicate that a current density of approximately 0.40 A/cm² provides an appropriate compromise between electrode area and energy consumption, resulting in electrode areas of 5.5 m² for pilot scale and 13,070 m² for industrial scale. This value is lower than the 0.6–0.7 A/cm² range reported by Beyrami et al. (2026), whereas Naeni et al. (2022) proposed even lower values (~0.18 A/cm²) to minimize $LCOH$. These differences confirm that optimal operating conditions remain highly system-dependent and strongly influenced by process integration, degradation assumptions, and economic criteria. The use of predictive degradation models could further improve the selection of optimal operating conditions for future works (Beyrami et al. 2026; Giridhar et al. 2024). The selected operating point was further validated using the proposed cost function derived from the parametric analysis. Figures 8a–b show the variation of the cost function at the industrial scale as functions of temperature and specific power consumption, with analogous trends observed at pilot scale. Increasing temperature and reducing current density decrease the objective function due to the strong dependence of operating costs on W_{SOEC}. Minimum costs are obtained under thermoneutral and mildly endothermic conditions, within 750–850 °C, corresponding to the typical commercial operating window for SOEC systems. Within this region, similar costs are obtained for i between 0.2 and 0.4 A/cm² at 800 °C, with the main differences associated with electrode area requirements. Therefore, 0.4 A/cm² was selected as the preferred operating point because it substantially reduces spatial requirements while maintaining relatively low energy consumption. Pressure has only a minor influence on the objective function, consistent with its limited effect on efficiency and electrical demand. Accordingly, operating conditions of 0.4 A/cm², 800 °C, and 1.4 bar provide a balanced compromise between efficiency, durability, and economic performance.



(a) Temperature (b) Specific energy consumption

Fig. 8 Variation of the cost function for high-temperature electrolysis at the industrial-scale system as a function of (a) temperature and (b) specific energy consumption.

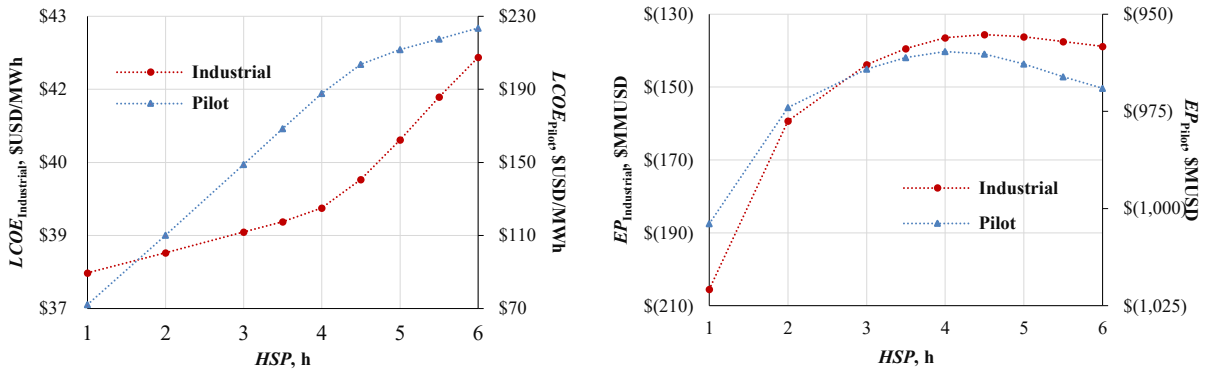
At pilot scale, the thermal energy required to heat the feed water to SOEC operating conditions is supplied through electrical resistance heating using PV electricity. At industrial scale, thermal energy is supplied by a natural gas-fired furnace, enabling comparison with conventional with conventional steam methane reforming (SMR). Considering representative Colombian natural gas from the Valle Medio del Magdalena (HHV = 41.02 MJ/m³, CH_4 = 77.06 mol%) (Vargas-Reyes et al. 2023), the production of 46.6 t H_2/day requires approximately 72 t/day of natural gas for heating, assuming 85% furnace efficiency. This corresponds to a hydrogen-to-natural-gas ratio of 0.65 t H_2/t natural gas, substantially higher than the 0.344 t H_2/t natural gas reported for a Colombian SMR unit (Martínez-González et al. 2024). When total natural gas consumption is considered, the SMR ratio decreases to 0.090 t H_2/t natural gas. Without the implemented heat integration strategy (Figures 3–4), the H_2-to-natural-gas ratio would decrease to approximately 0.3, highlighting the critical role of thermal integration in improving energy efficiency and reducing fuel consumption (Wang et al. 2021; Cheng et al. 2021). Industrial-scale operation produces CO_2 emissions associated with natural gas combustion. The estimated emission factor is 4.7 kg CO_2/kg H_2, based on the EPA emission factor of 53.06 kg CO_2/MMBTU (EPA 2025). This value remains lower than the 5.84 kg CO_2-eq/kg H_2 associated with electricity supply from the Colombian grid (Martínez-González et al. 2024), indicating that furnace-assisted heating may result in lower overall emissions than grid-dependent operation. Furthermore, the estimated emissions are substantially lower than the approximately 24.8 kg CO_2/kg H_2 (including combustion-related emissions) reported for conventional Colombian SMR systems (EPA 2025; IEA 2019b). Finally, increasing hydrogen recirculation raises the overall energy demand, because recycled hydrogen must be reheated from approximately 50 °C to 800 °C. As

shown in Figures 7–8, recirculation exerts only a minor influence on W_{SOEC} and electrode area, particularly at low temperatures. However, higher recycle fractions increase auxiliary heating requirements and sweep steam demand, thereby reducing overall process efficiency (InsightAce Analytic Pvt. 2023; Wang et al. 2019).

3.2 Photovoltaic systems. The electrical power requirements of the SOEC system ($\boldsymbol{W_{SOEC}}$), obtained from Aspen HYSYS simulations, are 0.0285 MW for the pilot-scale configuration and 65.31 MW for the industrial-scale configuration (Table 2). In addition to the electrolyser demand, the PV system must supply electricity to balance-of-plant (BOP) equipment, including compression, pumping, and auxiliary operations. At pilot scale, the PV system additionally supplies electrical heating and battery charging to enable stand-alone operation for up to 14 h. Under these conditions, the electrolyser accounts for approximately 29.5% and 86.9% of the total electricity demand at pilot and industrial scales, respectively. In the pilot-scale configuration, battery charging represents the dominant auxiliary demand (59.5%), followed by electrical heating (8%), and gas compression (4%). At industrial scale, compression contributes approximately 13% of the total electricity demand. Based on these requirements, the PV systems were sized at 931 panels (approximately 2,209 m^2) for pilot scale and 719,107 panels (approximately 1.71 km^2) for industrial scale, assuming $\boldsymbol{HSP}$ of 3.69 h and 10 h/day of operation. Figures 9a-b present the influence of $\boldsymbol{HSP}$ on $\boldsymbol{LCOE}$ and the proposed economic potential ($\boldsymbol{EP}$). Lower $\boldsymbol{HSP}$ values follow to larger PV capacities, thereby reducing $\boldsymbol{LCOE}$ due to increased electricity generation. Changes in $\boldsymbol{LCOE}$ slopes reflect the inverse relationship between panel number and $\boldsymbol{HSP}$. The higher curvature in $\boldsymbol{LCOE}$ for the pilot scale can be attributed to the battery storge requirements.

From an economic perspective, the optimal operating condition corresponds to the critical $\boldsymbol{HSP}$ ($\boldsymbol{HSP}$*) that maximizes EP function. The obtained values are $\boldsymbol{HSP}$* = 4.03 h for the pilot scale and $\boldsymbol{HSP}$* = 4.57 h for the industrial scale, corresponding to $LCOE$ values of approximately \$185.7 USD/MWh and \$39.7 USD/MWh, respectively. At $\boldsymbol{HSP}$*, the industrial-scale system requires 580,636 PV panels, resulting in an annual electricity deficit of 12.8 GWh and a surplus of 23.4 GWh, yielding a net positive balance of 10.6 GWh. Similarly, the pilot-scale configuration requires 852 panels, with an electricity deficit of 2.6 MWh and a surplus of 65 MWh, corresponding to a net positive balance of 62.4 MWh. Compared with the conservative design based on $\boldsymbol{HSP}$ = 3.69 h, operation at $\boldsymbol{HSP}$* reduces $CAPEX_{PV}$ by approximately \$24.5 MUSD at industrial scale and \$0.014 MUSD at pilot scale. For $\boldsymbol{HSP}$<$\boldsymbol{HSP}$*, $\boldsymbol{EP}$ decreases due to the substantial increase in PV capacity and investment cost, while for $\boldsymbol{HSP}$>$\boldsymbol{HSP}$*, $\boldsymbol{EP}$ decreases because electricity deficits become dominant. Consequently, $\boldsymbol{HSP}$=$\boldsymbol{HSP}$* was selected as the optimal design criterion for PV sizing. The resulting $LCOE$ values remain lower than those reported by the U.S.

Department of Energy ($47 USD/MWh without storage and $94 USD/MWh with storage) (Ramasamy et al. 2025; IRENA 2025), primarily due to the favorable solar irradiation conditions of Barrancabermeja.



(a) LCOE (b) Economic potential

Fig. 9 Variation of LCOH (a) and economic potential (b) as a function of HSP.

Table 4 compares the pilot-scale results of the present study with previous investigations based on PEM electrolysis systems (Zghaibeh et al. 2022; Jannati and Nazarpour 2017). Zghaibeh et al. (2022) reported a larger number of PV panels, despite excluding BOP electricity requirements, mainly because of higher H_2 production rates and the larger specific power consumption associated with PEM systems. Similarly, (Jannati and Nazarpour 2017) reported higher specific energy consumption and larger PV installation areas, although detailed panel specifications were no provided. Despite the lower H_2 production evaluated in the present work, the estimated PV area remains comparable to that reported in (Jannati and Nazarpour 2017), indicating the strong influence of local irradiation conditions and system assumptions on PV sizing. Compared with the photovoltaic pilot plant installed at RefiCar, the number of panels estimated for Barrancabermeja is approximately three times higher (Ecopetrol 2022). This difference is primarily attributed to the inclusion of BOP electricity demand and battery storage in the present study, together with the lower solar irradiation conditions of Barrancabermeja relative to Cartagena (IDEAM 2015). Table 4 additionally compares the industrial-scale results with previous studies. The obtained PV area is consistent with the values reported in (Bilgen 2001), which estimated an installation area of approximately 1.6 km² for a hydrogen production capacity of 8,333.3 t/year in Montreal using 0.666 kW panels and 2,000 h/year of operation. The larger installation area reported by Bilgen (2001) is mainly associated with the lower solar irradiation conditions of Montreal despite the lower hydrogen production capacity. The present results are also consistent with studies employing PEM

electrolysers (Zghaibeh et al. 2022; Henry et al. 2023). Regarding Zghaibeh et al. (2022), increasing the number of PV panels from 10,000 to 537,147 resulted in higher hydrogen production, consistent with the superior solar irradiation conditions reported for Salalah, Oman. Overall, these comparisons demonstrate that the proposed methodology provides physically and economically consistent results across different production scales and geographical conditions.

At industrial scale, the electricity generation required to produce 46.6 t/day of H_2 would increase Colombia's installed photovoltaic capacity from approximately 0.01 GW to 0.14 GW, thereby contributing to the decarbonization of the national electricity matrix. Regarding energy storage, the pilot-scale system requires 265 batteries operating a 14 h discharge capacity, arranged in four parallel rows (McCormick et al. 2016; Monforti-Ferrario et al. 2021). In contrast, the industrial-scale configuration would require approximately 350,560 batteries together with substantially larger PV installations. Due to the considerable space requirements, capital costs, and operational complexity associated with large-scale battery storage, electricity storage was excluded from the industrial-scale design.

Table 4. Comparison of results for the photovoltaic systems.

	H_2, kg/h	**Specific Power, kWh/kg H_2**	**Panels, (Wp)**	**Total Panel Area, m^2**	**I annual, kWh/m^2**
			Pilot scale		
This Work	0.83	33.50 (48.01)$^{\pm}$	763* (0.50 kW)	1,811	1,460–1,642
Zghaibeh et al. 2022	12.50	40.00	10,000 (0.50 kW)	------	2,337–2,483
Jannati and Nazarpour 2017	0.20	Max 56.36	------	1500	HSP=5.3
			Industrial Scale		
This Study	1,941.7	33.50 (47.84)$^{\pm}$	631,787* (0.50 kW)	1,499,230	1,460–1,642
Bilgen 2001	4,166.7	------	(0.666 kW)	1,600,000	--------
Henry et al. 2023	500.0	58.94–62.44	-------	-------	1,000
Zghaibeh et al. 2022	60.0	40.0	10,000 (0.50 kW)	-------	2,337–2,483

582 **Note**: ±Specific power consumption values consider the total electricity requirements reported in Table 2. For the
583 pilot-scale system, the total includes 9.6 kWh/kg H_2 for electrical heating of the feed water, 4.8 kWh/kg H_2 for
584 compression, and 0.015 kWh/kg H_2 for pumping. For the industrial-scale system, the total includes 9.15 kWh/kg H_2
585 for thermal heating, 5.04 kWh/kg H_2 for compression, and 0.017 kWh/kg H_2 for pumping. *The number of PV panels
586 was calculated based on the total electricity requirements (Table 2), an average solar irradiance availability of 10 h
587 per day, and an economic balance between incomed due to electricity surplus and investment costs (Figure 9). For the
588 pilot-scale system, the panels count additionally includes the capacity required to charge batteries to enable an
589 operating period of 14 h.

3.3 Costs and Financial Results. Table 5 summarizes the estimated ***CAPEX***, while Figure S6a presents the corresponding contributions after incorporating Colombian legal incentives. At pilot scale, the ***CAPEX*** associated with the PV system, electrolysis and BOP equipment, and total installed investment are estimated at $260.8 kUSD, $5,283.7 kUSD, and $4,662.6 kUSD, respectively. At industrial scale, these values increase to $100.7 MUSD, $1,310.9 MUSD, and $1,188.7 MUSD. Fiscal incentives reduce total ***CAPEX*** by approximately $885.9 kUSD at pilot scale and $225.9 MUSD at industrial scale, demonstrating the substantial influence of Colombian renewable-energy policies on project economics. BOP equipment constitutes the dominant ***CAPEX*** contribution, accounting for 92.2% and 79.1% of total investment at pilot and industrial scales, respectively, consistent with previous SOEC techno-economic studies (Cavalcanti et al. 2025; Jiménez-Martín et al. 2024; IRENA 2020). At pilot scale, compressors (36.7%) and heat-transfer equipment (29.3%) represent the largest capital contributors due to the relatively high impact of auxiliary equipment under low production rates. In contrast, industrial-scale ***CAPEX*** is dominated by oxygen storage systems (49.1%), highlighting the significant influence of large-scale O_2 handling and storage requirements on overall project economics. These results demonstrate that oxygen valorization cannot be decoupled from infrastructure investment when large-scale electrolysis systems are considered. Table 6 compares the normalized ***CAPEX*** contributions for both scales, including purification systems, storage infrastructure, and working capital. The specific present-value ***CAPEX*** associated with hydrogen production decreases from $59.70 USD/kg H_2 at pilot scale to $6.67 USD/kg H_2 at industrial scale, while the equivalent value for oxygen decreases from $7.74 USD/kg O_2 to $0.85 USD/kg O_2. Similarly, the normalized energy-based investment decreases from $205.02 kUSD/kW to $23.69 kUSD/kW. Overall, scaling the system from pilot to industrial operation reduces normalized investment costs by approximately 92%, confirming the strong economies of scale associated with integrated SOEC systems. Figures 10a–b illustrate the relative contributions of purification systems, product storage, and working capital to the normalized ***CAPEX*** values. At pilot scale, excluding O_2 purification and storage reduces the hydrogen-related normalized ***CAPEX*** by 23.4%, whereas excluding H_2-related systems reduces the oxygen-related ***CAPEX*** by 18.4%. At industrial scale, the influence of O_2-related infrastructure becomes substantially larger, reducing hydrogen-related ***CAPEX*** by approximately 40.1%. These results confirm that oxygen handling systems become increasingly relevant as production scale increases. Further exclusion of product storage and working capital leads to additional ***CAPEX*** reductions. At pilot scale, the hydrogen- and oxygen-related normalized ***CAPEX*** decrease by 41.0% and 36.7%, respectively. At industrial scale, the reductions become substantially more pronounced, reaching 71.1% for hydrogen and 42.6% for

oxygen. Therefore, storage systems and indirect capital contributions become dominant economic drivers for large-scale deployment.

Table 5. $CAPEX$ (kUSD) comparison between pilot- and industrial-scale production.[†]

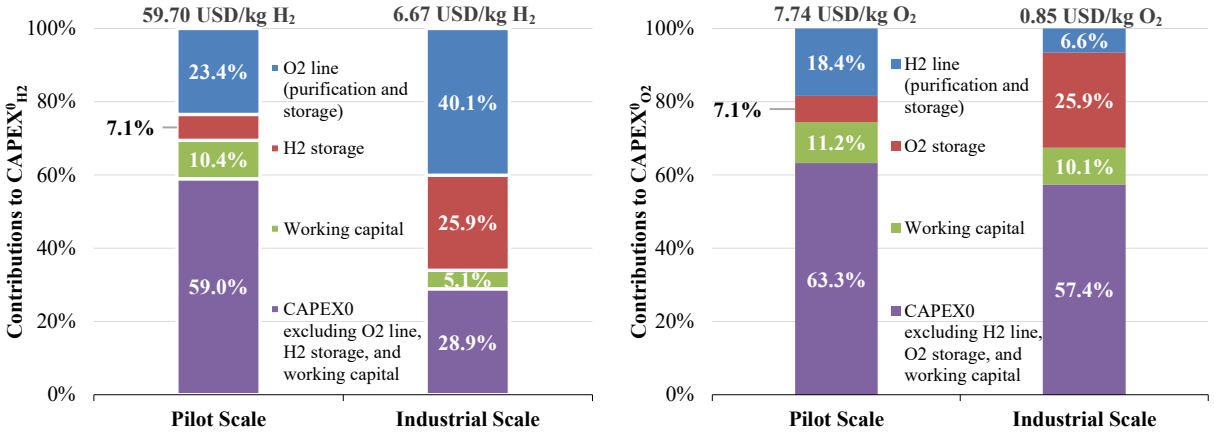
	Photovoltaic System	
	Pilot Scale	**Industrial Scale**
Panels	$ 127.8	$ 87,095.4
Batteries	$ 97.3	----
Converters	$ 1.6	$ 411.4
Charge control	$ 0.1	$ 23.9
Installation, 15%	$ 34.0	$ 13,129.6
Subtotal	$ 260.8	$ 100,660.3
	Electrolysis System	
	Pilot Scale	**Industrial Scale**
Electrolyser	$ 149.1 (Electrode area: 5.5 m^2)	$ 167,872.8 (Electrode area: 13,070 m^2)
Flash Tanks	$ 619.0 (8 tanks, D: 0.2–0.4 m, H: 1.2–2.2 m, t: 0.3–1.0 in)[*]	$ 26,622.5 (16 tanks, D: 1.2–4.0 m, H: 4.3–14.0 m, t: 0.3–3.0 in)[*]
H_2 Storage Tanks	$ 95.1 (V=8.6 m^3)[+]	$ 88,787.4 (V=20,060.3 m^3)[+]
O_2 Storage Tanks	$ 733.8 (V=4.2 m^3)[+]	$ 694,675.7 (V=9,918.4 m^3)[+]
Heat Exchangers and Heater	$ 1,626.6 (Q: 0.1–3.2 kW, Q_H: 8.2 kW, A: 0.2–0.8 m^2)[±]	$ 22,877.3 (Q: 0.1–7.5 MW, Q_H: 17.8 MW, A: 21–386 m^2)[±]
Compressors	$ 2,038.7 (11 compressors, Power: 0.15–6.2 kW)	$ 286,067.0 (11 compressors, Power: 0.3–1.5 MW)
Electrolyser Installation (12%)	$ 21.3	$ 23,972.2
Subtotal	$ 5,283.7	$1,310,875.1
Land	$ 4.1	$ 3,066.1
CAPEX without Incentives	$ 5,548.5	$1,414,601.5
VAT (19%)	$ 885.9	$ 225,860.7
CAPEX with Incentives	$ 4,662.6	$1,188,740.8

Note: [†]The calculated equipment costs already include direct and indirect plant costs, fixed capital investment, and working capital, as estimated using Lang's factor (Seider et al. 2017; Peters et al. 2002). [*]D, H, and t correspond to the internal diameter, height, and wall thickness of the tanks, respectively. [+]V corresponds to the volume of total storage system at 30 bar and 40°C. [±]Q represents the exchanged heat, whereas Q_H is the heat required to evaporate the inlet water supplied to the SOEC. A corresponds to the heat-exchanger area.

Table 6. Specific $CAPEX^0$ (with incentives) comparison between pilot- and industrial-scale production.[±]

Specific $CAPEX^0$	Pilot Scale	Industrial Scale
$\overline{CAPEX}^0_{H2}$, \$ USD/kg H_2	59.70	6.67
$\overline{CAPEX}^0_{H2}{}^{\dagger}$, \$ USD/kg H_2	45.71	4.00
$\overline{CAPEX}^0_{H2}{}^{\dagger+}$, \$ USD/kg H_2	41.45	2.27
$\overline{CAPEX}^0_{H2}{}^{\dagger+\ddagger}$, \$ USD/kg H_2	35.23	1.93
$\overline{CAPEX}^0_{O2}$, \$ USD/kg O_2	7.74	0.85
$\overline{CAPEX}^0_{O2}{}^{*}$, \$ USD/kg O_2	6.31	0.80
$\overline{CAPEX}^0_{O2}{}^{*+}$, \$ USD/kg O_2	5.76	0.58
$\overline{CAPEX}^0_{O2}{}^{*+\ddagger}$, \$ USD/kg O_2	4.89	0.49
$\overline{CAPEX}^0_{kW}$, \$ kUSD/kW	205.02	23.69
$\overline{CAPEX}^0_{kW}{}^{\dagger}$, \$ kUSD/kW	156.97	14.20
$\overline{CAPEX}^0_{kW}{}^{\dagger+}$, \$ kUSD/kW	142.33	8.05
$\overline{CAPEX}^0_{kW}{}^{\dagger+\ddagger}$, \$ kUSD/kW	120.97	6.84

Note: $^{\pm}\overline{CAPEX}^0_{H2}$: $CAPEX$ expressed in present value per unit of total produced H_2 expressed in present value. $\overline{CAPEX}^0_{O2}$: $CAPEX$ expressed in present value per unit of total produced O_2 expressed in present value. $\overline{CAPEX}^0_{kW}$: $CAPEX$ expressed in present value per unit of total produced power based on LHV, expressed in present value. $^{\dagger}CAPEX$ excluding equipment required for O_2 purification and storage. $^{*}CAPEX$ excluding equipment required for H_2 purification and storage. $^{+}CAPEX$ excluding product storage. $^{\ddagger}CAPEX$ excluding working capital.



(a) $CAPEX^0$ per mass of H_2 (b) $CAPEX^0$ per mass of O_2

Fig. 10 Contributions to specific $CAPEX^0$ with incentives.

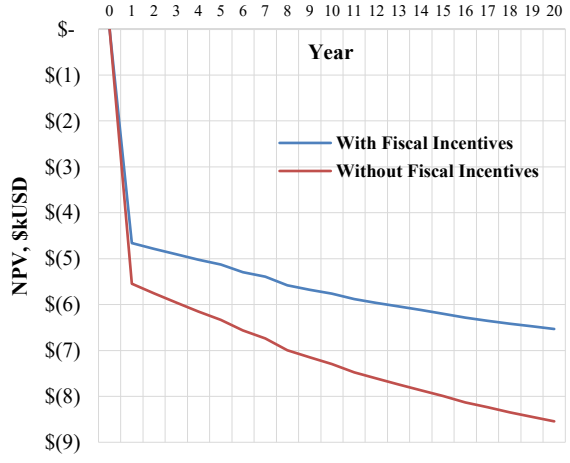
Table 7 summarizes the first-year $\boldsymbol{OPEX}$, while Figure S6b presents the corresponding contributions after applying fiscal incentives. Total $\boldsymbol{OPEX}$ is estimated at \$526.2 kUSD for the pilot-scale configuration and \$57.2 MUSD for industrial operation. The $\boldsymbol{OPEX}$ structure changes substantially with production scale. At pilot scale, direct labor, benefits, and wages (DB&W) dominate operating costs, accounting for approximately 83.0% of total $\boldsymbol{OPEX}$. Conversely, at industrial scale, operation and maintenance (O&M) costs and electricity consumption become the dominant contributors, representing 44.5% and 33.9%, respectively. Simultaneously, the relative contribution of labor decreases to only 4.6%, reflecting the improved labor efficiency associated with large-scale continuous operation. Normalized operating costs decrease substantially with scale-up. The $\boldsymbol{OPEX}$ per installed power decreases from \$18.14 kUSD/kW to \$0.88 kUSD/kW, while the $\boldsymbol{OPEX}$ per unit hydrogen production decreases from \$77.0 USD/kg H_2 to \$3.6 USD/kg H_2. These reductions confirm the strong economies of scale associated with industrial SOEC deployment. The $\boldsymbol{OPEX}/\boldsymbol{CAPEX}$ ratio decreases from 12.4% at pilot scale (10.8% without incentives) to 4.8% at industrial scale (4.6% without incentives), remaining consistent with values reported in the literature (Christensen 2020). Additional reductions could potentially be achieved through hybrid electricity supply strategies combining photovoltaic generation with grid integration (Lähdemäki 2021).

Table 7. Comparison of first-year $OPEX$ between pilot- and industrial-scale production.

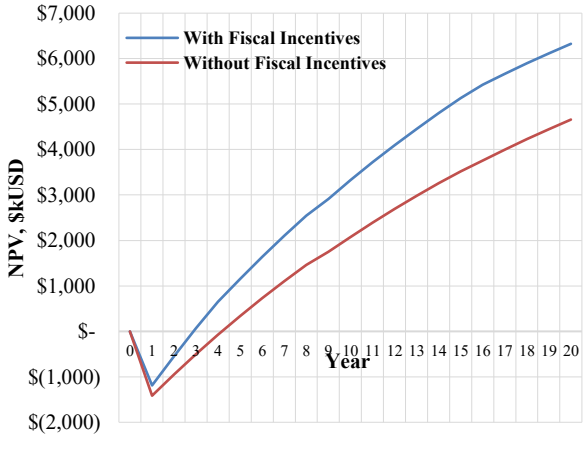
		Photovoltaic System, \$kUSD	
		Pilot Scale	**Industrial Scale**
O&M, 2%		\$ 5.2	\$ 2,013.2
	Subtotal	\$ 5.2	\$ 2,013.2
		Electrolysis and BOP Systems, \$kUSD	
		Pilot Scale	**Industrial Scale**
Electricity (\$0.062 USD/kWh)		\$ 0.16 (2600 kWh/year)	\$ 23,077.1 (320.9 GWh/year)
Water (\$0,07 USD/kGal)		\$ 0.04 (586.0 kGal/year)	\$ 104.6 (1,560.5 MGal/year)
Natural gas (\$0,08 USD/kWh)		------	\$ 11,512.9 (145.7 GWh/year)
O&M, 2%		\$ 101.0	\$ 28,292.0
	Subtotal	\$ 101.2	\$ 62,986.6
	DB&W	\$ 436.8	\$ 2,620.8

Total without Incentives	$ 543.2	$ 67,620.6
VAT	$ 17.0	$ 10,378.1
Total with Incentives	$ 526.2	$ 57,242.5

Figures 11a–b compare the cumulative NPV evolution for scenarios with and without legal incentives. Under the assumed selling prices of \$10 USD/kg H_2 and \$5 USD/kg O_2, the pilot-scale configuration remains economically infeasible throughout the project lifetime, with cumulative NPV remaining negative. In contrast, the industrial-scale configuration exhibits sustained positive NPV growth, confirming economic viability. Fiscal incentives substantially improve industrial-scale profitability. Accelerated depreciation during the first three years and reduced income tax rates increase cumulative NPV by approximately 34.2% relative to the non-incentivized scenario and reduce the payback period from 4.2 to 2.9 years. Table 8 summarizes the main financial indicators. The $CAPEX$ values estimated in the present work exceed those reported in previous studies (Zghaibeh et al. 2022; Jang et al. 2022; Velasquez-Jaramillo et al. 2024; León et al. 2023; Khan et al. 2021a-b; Perna et al. 2022; Sánchez-Squella et al. 2025), primarily because the proposed methodology incorporates product purification and storage systems, working capital, direct and indirect costs through the Lang factor methodology, and explicit oxygen valorization infrastructure. At pilot scale, the combination of high normalized $CAPEX$ and $OPEX$ results in elevated levelized costs and negative NPV. In contrast, industrial-scale deployment achieves an $LCOH$ of \$9.65 USD/kg H_2, within the upper range reported for renewable high-temperature electrolysis systems, together with positive NPV and high IRR. These findings demonstrate that large-scale integration is essential to achieve economic viability under current technological and market conditions.



(a) Pilot-scale configuration



(b) Industrial-scale configuration

Fig. 11 Cumulative NPV at the pilot and industrial-scales configurations.

The industrial-scale IRR reaches 58.4%, substantially exceeding the $WACC_{real}$ (5.5%), thereby confirming strong investment attractiveness. Similarly, PI reaches 6.49, indicating robust long-term profitability. Scale-up substantially reduces all levelized costs. When incentives are included, the $LCOE$ decreases from \$82.19 USD/MWh at pilot scale to \$35.39 USD/MWh at industrial scale. Similarly, the $LCOH$ decreases from \$118.01 USD/kg H_2 to \$9.65 USD/kg H_2, while $LCOO$ decreases from \$15.76 USD/kg O_2 to \$2.40 USD/kg O_2. Without incentives, the corresponding values increase to \$99.81 USD/MWh, \$144.00 USD/kg H_2, and \$19.13 USD/kg O_2 at pilot scale, and to \$43.14 USD/MWh, \$13.18 USD/kg H_2, and \$3.42 USD/kg O_2 at industrial scale. Consequently, fiscal incentives reduce $LCOE$, $LCOH$, and $LCOO$ by approximately 18–30%, demonstrating their critical role in enabling financial feasibility for renewable hydrogen systems in Colombia.

Table 8. Comparison of financial indices between pilot- and industrial-scale productions.

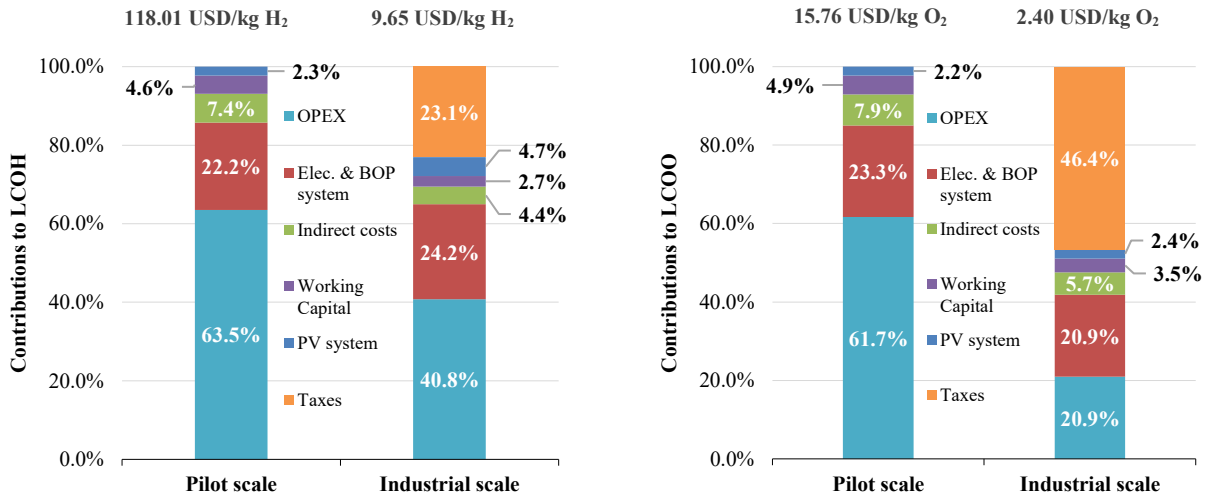
Ref.	Annual Production, GWh (t H_2)	Energy Source	Elect. (%ef.)	P*, bar	CAPEX, \$MUSD (OPEX, \$MUSD/year)	Storage, % on CAPEX	Selling Prices, \$USD/kg H_2 (\$USD/kg O_2)	LCOH, \$USD/kg H_2 (LCOE, \$UDS/MWh)	NPV, \$MUSD (IRR, %)
Pilot Scale									
This work	0.228 (6.83)	PV and batteries	SOEC (82.2)	1.4 (30.0)	4.25 (0.53)	6.6%	10.0 (5.0)	118.01 (82.19)	-6.59 (0<)
Jiménez-Martín et al. 2025	0.044 (1.23)	PV	PEM	7.0 (350)	0.075 (0.006)	3.3%	6.0 (0.03)	6.13 (57.1)	-0.05 (0<)
	0.11 (2.45)	PV	PEM	7.0 (350)	2.21 (0.168)	3.6%	6.0 (0.03)	5.63 (48.5)	0.38 (14%)
Cavalcanti et al. 2025	0.420 (15.0)	PV and batteries	SOEC	1.0 (----)	25.6 (----)	----	----	9.42 (----)	---
Jang et al. 2022	2.69 (80.76)	Grid	SOEC (61.4)	----	0.939 (0.365)	----	7.5 – 9.0	10.16	0< (----)
Zghaibeh et al. 2022	3.03 (90.91)	PV	PEM	----	5.726 (0.202)	----	10.8	6.7 (----)	6.025 (----)
Perna et al. 2022	8.93 (150.0)	PV and Grid	PEM (56.0)	900	7.238 (0.843)	----	11.51	8.55 (----)	6.653 (40%)
Industrial Scale									

This work	268,72 (15,921.7)	PV and Grid	SOEC (82.2)	1.4 (30.0)	1,188.7 (57.2)	55.4	10.0 (5.0)	9.65 (35.39)	6,526.2 (58.4)
Velasquez-Jaramillo et al. 2024	258.15 (19,981.0)	PV	PEM (80%)	----	185.5 (----)	----	14.0	8.43 (38.7)	180.0 (18)
León et al. 2023	161.64 (1,000.0)	PV	AWE	----	48.39 (7.02)	----	>11.0	7.0 (----)	>0.0 (>4.0)
Khan et al. 2021a	776.97 (16,650.0)	PV	AWE (70%)	20 (----)	464.33 (8.91)	----	>5.9	4.9 (----)	>0 (>12.0)

* Pressure of electrolyser. Storage pressure in parenthesis.

Figures 12a–b present the percentage contributions to $LCOH$ and $LCOO$ at both scales. At pilot scale, $OPEX$ dominates both levelized costs due to the low production capacity and high relative labor costs. Tax contributions are absent because negative cash flows prevent taxable income generation. At industrial scale, the contribution structure changes substantially. $OPEX$ remains important, but taxes and capital recovery become increasingly relevant due to the positive profitability of the project. The tax contribution to $LCOO$ is larger than that associated with $LCOH$ because oxygen production volumes are substantially higher than hydrogen production volumes. Without incentives, the tax contribution to $LCOH$ increases from \$2.23 to \$3.75 USD/kg H_2, while the equivalent contribution to $LCOO$ increases from \$1.11 to \$1.87 USD/kg O_2. Similarly, $OPEX$ contributions increase from \$74.95 to \$89.45 USD/kg H_2 and from \$9.72 to \$11.60 USD/kg O_2 at pilot scale. At industrial scale, the corresponding increases are substantially smaller, further confirming the economic advantages associated with large-scale deployment.

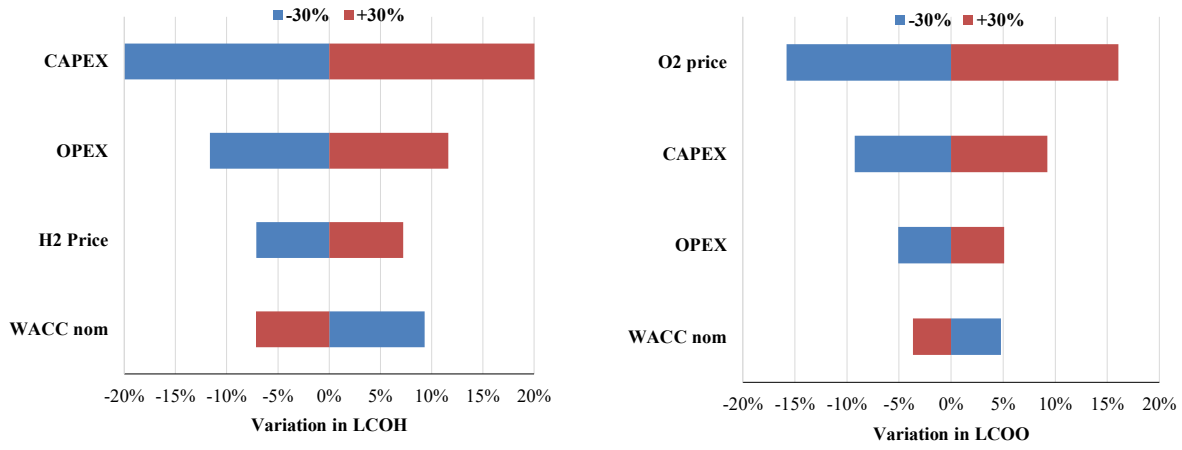
3.4 Sensitivity Analysis Results. Figures 13a–b present the sensitivity of $\boldsymbol{LCOH}$ and $\boldsymbol{LCOO}$ to ±30% variations in key economic parameters, including $\boldsymbol{CAPEX}$, $\boldsymbol{OPEX}$, product selling price, and $\boldsymbol{WACC_{nom}}$. For $\boldsymbol{LCOH}$ (Figure 13a), $\boldsymbol{CAPEX}$ exerts the strongest influence, producing variations of approximately ±20% relative to the base-case value. $\boldsymbol{OPEX}$ and hydrogen selling price exhibit the second-largest effects, confirming that both investment cost and operational expenditures remain the dominant economic drivers of photovoltaic-powered SOEC systems. In contrast, $\boldsymbol{WACC_{nom}}$ shows a comparatively smaller influence on $\boldsymbol{LCOH}$. The inverse trend observed for $\boldsymbol{WACC_{nom}}$ arises from the interaction between discounted cash flows, taxation, and annualized production costs within the adopted financial framework. For $\boldsymbol{LCOO}$ (Figure 13b), oxygen selling price becomes the most influential parameter, followed by $\boldsymbol{CAPEX}$ and $\boldsymbol{OPEX}$. Similar to the $\boldsymbol{LCOH}$ behavior, $\boldsymbol{WACC_{nom}}$ exhibits a comparatively smaller effect on $\boldsymbol{LCOO}$. These results demonstrate that oxygen commercialization substantially influences the economic performance of integrated hydrogen–oxygen production systems, particularly at large production scales where oxygen generation becomes significant.



(a) $LCOH$ (b) $LCOO$

Fig. 12 Percentage contributions to LCOH and LCOO with legal incentives

Overall, the sensitivity analysis confirms that capital investment and product commercialization strategies constitute the primary determinants of economic feasibility. Consequently, future reductions in ***LCOH*** will likely depend on simultaneous improvements in electrolyser manufacturing cost, photovoltaic deployment, infrastructure integration, and product market development.



(a) $LCOH$ (b) $LCOO$

Fig. 13 Sensitivity analysis of LCOH and LCOO to ±30% variations in key economic parameters.

The proposed methodology additionally provides insight into the feasibility of achieving the hydrogen cost targets established in Colombia's Hydrogen Roadmap (Minenergía 2021). Under the base-case industrial scenario evaluated in this study, the system achieves an $LCOH$ of approximately \$9.65 USD/kg H_2, assuming a hydrogen selling price of \$10 USD/kg H_2 and explicit oxygen valorization. Therefore, reaching the national target of \$1.7 USD/kg H_2 by 2030 would require a reduction of nearly 82% in levelized hydrogen cost. Such a reduction appears highly challenging under current technological and economic conditions, particularly considering the high capital intensity associated with SOEC systems, storage infrastructure, and photovoltaic deployment. Achieving this target would require simultaneous progress in multiple areas, including large-scale electrolyser manufacturing, reductions in photovoltaic and storage costs, improved stack durability, lower electricity costs, enhanced thermal integration, and expanded fiscal incentives. Nevertheless, the present results suggest that intermediate $LCOH$ values in the range of \$5–7 USD/kg H_2 could become attainable under optimistic scenarios combining technological learning, economies of scale, and sustained policy support. In this context, Colombia's favorable solar irradiation conditions and existing industrial infrastructure provide important competitive advantages for future hydrogen deployment. The analysis also highlights the strategic role of oxygen valorization in improving overall project economics. Since oxygen is generated

in large quantities during electrolysis, its commercialization in industrial and medical markets provides an additional revenue stream capable of partially offsetting both $\boldsymbol{CAPEX}$ and $\boldsymbol{OPEX}$. As demonstrated by the sensitivity analysis, oxygen selling price strongly affects $LCO\boldsymbol{O}$ and indirectly improves hydrogen production economics, particularly at industrial scale. Therefore, oxygen purification, storage, and commercialization should not be treated as secondary process components but rather as integral elements of the techno-economic design of large-scale green hydrogen systems. The results demonstrate that integrated hydrogen–oxygen production frameworks can significantly improve the economic competitiveness of photovoltaic-driven electrolysis systems in emerging hydrogen markets such as Colombia.

Conclusions

This study presented the first techno-economic assessment in Colombia to explicitly incorporate oxygen co-product valorization into the evaluation of photovoltaic-powered solid oxide electrolysis cell (SOEC) systems for green hydrogen production. The proposed framework integrated process simulation, photovoltaic system sizing, and detailed financial analysis, including balance-of-plant (BOP) equipment, product storage, and Colombian fiscal incentives, for both pilot- and industrial-scale configurations in Barrancabermeja. From a technical perspective, the results confirmed the feasibility of coupling photovoltaic energy with high-temperature SOEC technology to produce high-purity hydrogen (99.8 vol%) and oxygen (99.6 vol%) at approximately 800 °C and pressures up to 30 bar. The process exhibited specific electrical energy consumption values consistent with reported SOEC performance Furthermore, the analysis of thermoneutral operation highlighted the strong influence of temperature, current density, and thermal integration on system efficiency and overall energy demand. The economic assessment identified production as the dominant factor governing project feasibility. At pilot scale, high normalized $\boldsymbol{CAPEX}$ and $\boldsymbol{OPEX}$ resulted in elevated $LCOH$ values and negative NPV, preventing economic viability. In contrast, industrial-scale deployment substantially reduced normalized investment and operating costs, leading to positive NPV, high IRR, and shorter payback periods. The obtained $LCOH$ values remained within the upper range reported for renewable high-temperature electrolysis systems under current technological conditions. The cost breakdown analysis revealed that BOP equipment and storage infrastructure dominate total capital investment, particularly at industrial scale, emphasizing the importance of incorporating auxiliary systems into techno-economic evaluations. In addition, oxygen purification, storage, and commercialization significantly improved overall economic performance, demonstrating

759 that oxygen valorization should be considered an integral component of large-scale electrolysis projects rather than as
760 a secondary by-product strategy. The incorporation of Colombian fiscal incentives further enhance project profitability
761 by reducing $\boldsymbol{CAPEX}$, lowering levelized costs, and shortening payback periods. Sensitivity analysis showed that
762 $\boldsymbol{CAPEX}$ and product selling prices are the most influential economic variables, whereas financing conditions exert a
763 comparatively smaller effect. Overall, the results indicate that economically competitive green hydrogen production
764 in Colombia will require large-scale deployment, continued reductions in electrolyser and photovoltaic costs, strong
765 policy support, and integrated hydrogen–oxygen commercialization strategies. The methodology developed in this
766 work provides a scalable and engineering-oriented framework for assessing green hydrogen projects in emerging
767 markets with favorable renewable-energy resources and can support future planning, and policy decisions associated
768 with the energy transition.

769 **Supplementary Data**

770 Figures showing PFDs for H_2 and O_2 generation at the pilot scale, electrolysis efficiency, energy
771 consumption, electrode area variation, and $CAPEX$ and $OPEX$ contributions.

772 **References**

773 Abad D, Vega F, Navarrette B, Delgado A, Nieto, E (2021) Modeling and simulation of an integrated power-to-
774 methanol approach via high temperature electrolysis and partial oxy-combustion technology. Int J Hydrogen Energy
775 46:34128-34147. https://doi.org/10.1016/j.ijhydene.2021.04.029

776 Abe JO, Popoola API, Ajenifuja E, Popoola OM (2019) Hydrogen energy, economy and storage: review and
777 recommendation. Int J Hydrogen Energy 44:15072-15086. https://doi.org/10.1016/j.ijhydene.2019.04.068

778 Abomazid AM, El-Taweel NA, Farag HEZ (2022) Optimal energy management of hydrogen energy facility using
779 integrated battery energy storage and solar photovoltaic systems. IEEE Trans Sustain Energy 13:1457–1468.
780 https://doi.org/10.1109/tste.2022.3161891

781 Agbadaola O, Qadir D, Ahmad F, et al. (2024) Hydrogen technologies and policies for sustainable future: A review.
782 Chem Pap. https://doi.org/10.1007/s11696-024-03403-8

783 Aldersey-Williams J, Rubert T (2019) Levelised cost of energy: A theoretical justification and critical assessment.
784 Energy Policy 124:169–179. https://doi.org/10.1016/j.enpol.2018.10.004

785 Arias-Gaviria J, Carvajal-Quintero SX, Arango-Aramburo S (2019) Understanding dynamics and policy for renewable
786 energy diffusion in Colombia. Renew Energy 139:1111–1119. https://doi.org/10.1016/j.renene.2019.02.138

787 Awad M, Said A, Saad MH, Farouk A, Mahmoud MM, Alshammari MS, Alghaythi ML, Abdel Aleem SHE,
788 Abdelaziz AY, Omar AI (2024) A review of water electrolysis for green hydrogen generation considering
789 PV/wind/hybrid/hydropower/geothermal/tidal and wave/biogas energy systems, economic analysis, and its
790 application. Alex Eng J 87:213–239. https://doi.org/10.1016/j.aej.2023.12.032

791 Barthelemy H, Weber M, Barbier F (2017) Hydrogen storage: Recent improvements and industrial perspectives. Int J
792 Hydrogen Energy 42:7254–7262. https://doi.org/10.1016/j.ijhydene.2016.03.178

793 Benalcazar P, Komorowska A (2024) Techno-economic analysis and uncertainty assessment of green hydrogen
794 production in future exporting countries. Renew Sustain Energy Rev 199:114512.
795 https://doi.org/10.1016/j.rser.2024.114512

796 Betancur S, Ortega-Avila N, López-Vidaña EC (2023) Strengths, weaknesses, opportunities, and threats analysis for
797 the strengthening of solar thermal energy in Colombia. Resources 13:3. https://doi.org/10.3390/resources13010003

798 Beyrami J, Nakashima RN, Nemati A, Frandsen HL (2026) Economic optimization of modular solid oxide electrolysis
799 system considering degradation and lifetime. Energy Convers Manag 348:120782.
800 https://doi.org/10.1016/j.enconman.2025.120782

801 Bilgen E (2001) Solar hydrogen from photovoltaic-electrolyser systems. Energy Convers Manag 42:1047–1057.
802 https://doi.org/10.1016/S0196-8904(00)00131-X

803 Blair et al. (2018) SystemAdvisorModel (SAM) General Description (Version 2017.9.5), NREL/TP-6A20-70414.
804 https://sam.nrel.gov/download.html

805 Bui T, Lee D, Ahn KY, Kim YS (2023) Techno-economic analysis of high-power solid oxide electrolysis cell system.
806 Energy Convers Manag 278:116704. https://doi.org/10.1016/j.enconman.2023.116704

807 Bukar AL, Chaitusaney S, Kawabe K (2024) Optimal design of on-site PV-based battery grid-tied green hydrogen
808 production system. Energy Convers Manag 307:118378. https://doi.org/10.1016/j.enconman.2024.118378

Burdack A, Duarte-Herrera L, López-Jiménez G, Polklas T, Vasco-Echeverri O (2023) Techno-economic calculation of green hydrogen production and export from Colombia. Int J Hydrogen Energy 48:1685–1700. https://doi.org/10.1016/j.ijhydene.2022.10.064

Ríos C, Molina PM, Brey JJ (2024) Simulation of the optimal plant size to produce renewable hydrogen based on the available electricity. Int J Hydrogen Energy 52:1325–1337. https://doi.org/10.1016/j.ijhydene.2023.08.306

Cavalcanti EJC, Rufino CTF, Lima AAS, Azevedo JLB (2025) Model, energy and economic analyses of solid oxide electrolysis cells for clean hydrogen production. Renew Energy 254:123747. https://doi.org/10.1016/j.renene.2025.123747

ChemEng. (2026) Economic Indicators: May 2026. https://www.chemengonline.com/economic-indicators-may-2026/?utm_source=related-articles&utm_medium=Related&utm_campaign=Related&utm_content=Related&utm_term=Related

Chen C, Xia Q, Feng S, Liu Q (2021) A Novel Solar Hydrogen Production System Integrating High Temperature Electrolysis with Ammonia Based Thermochemical Energy Storage. Energy Convers Manag 237:114143. https://doi.org/10.1016/j.enconman.2021.114143

Christensen, A (2020) Assessment of Hydrogen Production Costs from Electrolysis: United States and Europe. International Council on Clean Transportation. https://theicct.org/sites/default/files/publications/final_icct2020_assessment_of_hydro

COM (2020) A hydrogen strategy for a climate-neutral Europe. Communication from the commission to the European parliament, the council, the European economic and social committee and the committee of the regions. https://ec.europa.eu/energy/sites/ener/files/hydrogen_strategy.pdf

CONPES-3934 (2018) Departamento Nacional de Planeación. Política de crecimiento verde. https://colaboracion.dnp.gov.co/cdt/conpes/económicos/3934.pdf

Council (2019) The Strategic Road Map for Hydrogen and Fuel Cells - Industry-academia-government action plan to realize a “Hydrogen Society” -. Hydrogen and Fuel Cell Strategy Council. Japan. https://www.meti.go.jp/english/press/2019/pdf/0312_002b.pdf

834 CREG (2021) Resolución 215 de 2021 por la cual se modifica la tasa de retorno para la actividad de distribución de
835 energía eléctrica, aprobada en la Resolución CREG 016 de 2018
836 https://gestornormativo.creg.gov.co/gestor/entorno/docs/resolucion_creg_0215_2021.htm

837 Eckl F, Moita A, Castro R, Neto RC (2025) Valorization of the by-product oxygen from green hydrogen production:
838 A review. Appl Energy 378:124817. https://doi.org/10.1016/j.apenergy.2024.124817

839 Ecopetrol (2022) El grupo Ecopetrol inició la producción de hidrógeno verde en Colombia.
840 https://www.ecopetrol.com.co/wps/portal/Home/es/noticias/detalle/Noticias+2021/el-grupo-ecopetrol-inicip-la-
841 produccion-de-hidrogeno-verde-en-colombia

842 EPA (2025) GHG Emission Factors Hub. United States Environmental Protection Agency.
843 https://www.epa.gov/climateleadership/ghg-emission-factors-hub

844 Erazo-Cifuentes YA, Orejuela JP, Manotas-Duque DF (2022) Technoeconomic comparison of scenarios for the
845 configuration of the renewable hydrogen supply chain in Colombia. Int J Energy Econ Policy 12:293–304.
846 https://doi.org/10.32479/ijeep.13576

847 FCH (2019a) Hydrogen roadmap. Europe. A sustainable pathway for the European energy transition. Fuel Cells and
848 Hydrogen 2 Joint Undertaking (FCH 2JU). Belgium.
849 https://www.fch.europa.eu/sites/default/files/Hydrogen%20Roadmap%20Europe_Report.pdf

850 FCH (2019b) Opportunities for Hydrogen Energy Technologies Considering the National Energy and Climate Plans.
851 Fuel Cells and Hydrogen 2 Joint Undertaking (FCH 2JU). Netherlands.
852 https://www.fch.europa.eu/sites/default/files/file_attach/Brochure%20FCH%20Netherlands%20%28ID%209474122
853 %29.pdf

854 FENOGE. (2023) Proyectos de Hidrógeno en Colombia. Fondo de Energías No Convencionales y Gestión Eficiente
855 de la Energía. Ministerio de Minas y Energía. https://fenoge.gov.co/documentos-
856 pdf/proyectos/Proyectos_Colombia_Hidrogeno3.pdf

857 Ferrero D, Lanzini A, Santarelli M, Leone P (2013) A comparative assessment on hydrogen production from low- and
858 high-temperature electrolysis. Int J Hydrogen Energy 38:3523–3536. https://doi.org/10.1016/j.ijhydene.2013.01.065

Fontalvo VM, Nelson GJ, Pupo-Roncallo O, Sanjuan ME, Gómez HA (2023) A techno-economic assessment for fuel cells hybrid systems in stationary applications. Int J Sustain Energy 42:889–912. https://doi.org/10.1080/14786451.2023.2244605

Gaikwad PS, Mondal K, Shin YK, et al. (2023) Enhancing the Faradaic efficiency of solid oxide electrolysis cells: Progress and perspective. NPJ Comput Mater 9:149. https://doi.org/10.1038/s41524-023-01044-1

García-García J, Sarmiento-Ariza Y, Campos-Rodríguez L, Rey-López J, Osma-Pinto G (2023) Evaluation of tax incentives on the financial viability of microgrids. Appl Energy 329:120293. https://doi.org/10.1016/j.apenergy.2022.120293

Garcia-Vallejo MC, Cardona Alzate CA (2024a) Prefeasibility analysis of biomass gasification and electrolysis for hydrogen production. Environ Res 248:118003. https://doi.org/10.1016/j.envres.2023.118003

Garcia-Vallejo MC, Cardona Alzate CA (2024b) Sustainability of hydrogen production considering alternative technologies towards a neutral carbon society. Int J Hydrogen Energy 64:853–863. https://doi.org/10.1016/j.ijhydene.2024.03.328

Ghezel-Ayagh H (2023) Solid Oxide Electrolysis System Demonstration DE-EE0009290 DOE Hydrogen Program 2023 Annual Merit Review and Peer Evaluation Meeting Project ID# TA039. https://www.hydrogen.energy.gov/docs/hydrogenprogramlibraries/pdfs/review23/ta039_ghezel-ayagh_2023_o-pdf.pdf

Giorgianni M, Nicita A, Maggio G (2025) Economic and business model analysis for hydrogen–oxygen co-production in hospitals. J Renew Sustain Energy 17:043301. https://doi.org/10.1063/5.0273144

Giridhar NV, Allan DA, Li M, Zitney SE, Biegler LT, Bhattacharyya D (2024) Optimal operation of solid-oxide electrolysis cells considering long-term chemical degradation. Energy Convers Manag 319:118950. https://doi.org/10.1016/j.enconman.2024.118950

Gniewomir F, Ghassan W (2023) Solid Oxide Electrolysis: A Technology Status Assessment. Clean Air Task Force. https://cdn.catf.us/wp-content/uploads/2023/11/15092028/solid-oxide-electrolysis-report.pdf

Gutiérrez-Martín F, Amodio L, Pagano M (2020) Hydrogen production by water electrolysis and off-grid solar PV. Int J Hydrogen Energy. https://doi.org/10.1016/j.ijhydene.2020.09.098

885 Guzman L, Henao A (2022) Are the current incentives sufficient to drive the use of solar PV in the Colombian
886 residential sector? An analysis from the perspective of game theory. Energy Strategy Rev 40:100816.
887 https://doi.org/10.1016/j.esr.2022.100816

888 Harboe S, Schreiber A, Margaritis N, Blum L, Guillon O, Menzler NH (2020) Manufacturing cost model for planar 5
889 kWel SOFC stacks at Forschungszentrum Jülich. Int J Hydrogen Energy 45:8015–8030.
890 https://doi.org/10.1016/j.ijhydene.2020.01.082

891 Hauch A, Küngas R, Blennow P, Hansen AB, Hansen JB, Mathiesen BV, Mogensen MB (2020) Recent advances in
892 solid oxide cell technology for electrolysis. Science 370:eaba6118. https://doi.org/10.1126/science.aba6118

893 Hauck M, Herrmann S, Spliethoff H (2017) Simulation of a reversible SOFC with Aspen Plus. Int J Hydrogen Energy
894 42:10329–10340. https://doi.org/10.1016/j.ijhydene.2017.01.189

895 Henbest S, Giannakopoulou E, Zindler E, Wu J, Rooze J, Chase J, Hostert D, Van Houten J (2021) New energy
896 outlook 2021: Long-term projections of the global energy sector. Bloomberg New Energy Finance.
897 https://www.bloomberg.com/company/new-energy-outlook/

898 Henry A, McStay D, Rooney D, Robertson PKJ, Foley A (2023) Techno-economic analysis to identify the optimal
899 conditions for green hydrogen production. Energy Convers Manag 291:117230.
900 https://doi.org/10.1016/j.enconman.2023.117230

901 Hinkley J, Hayward J, McNaughton R, Gillespie R (2016) Cost assessment of hydrogen production from PV and
902 electrolysis. Report to ARENA as part of Solar Fuels Roadmap, Project A-3018.
903 https://arena.gov.au/assets/2016/05/Assessment-of-the-cost-of-hydrogen-from-PV.pdf

904 Houchins C, James BD, Acevedo Y, Watts Z (2022) Hydrogen storage system cost analysis (2017–2021). Final report.
905 https://www.osti.gov/servlets/purl/1975554

906 Hu K, Fang J, Ai X, Huang D, Zhong Z, Yang X, Wang L (2022) Comparative study of alkaline water electrolysis,
907 proton exchange membrane water electrolysis and solid oxide electrolysis through multiphysics modeling. Appl
908 Energy 312:118788. https://doi.org/10.1016/j.apenergy.2022.118788

ICONTEC (2008) NTC 1671: Gas cylinders for medical use. Marking for identification of content. https://tienda.icontec.org/gp-cilindros-de-gas-de-uso-medico-marcado-para-la-identificacion-del-contenido-ntc1671-2008.html

IDEAM (2015) Atlas de radiación solar de Colombia–Interactivo. http://atlas.ideam.gov.co/visorAtlasRadiacion.html

IEA (2019a) World energy outlook 2019. International Energy Agency, Paris. https://www.iea.org/reports/world-energy-outlook-2019

IEA (2019b) The future of hydrogen. International Energy Agency, Paris. https://www.iea.org/reports/the-future-of-hydrogen

IEA (2023) Emissions from oil and gas operations in net zero transitions: A World Energy Outlook special report on the oil and gas industry and COP28. OECD Publishing, Paris. https://doi.org/10.1787/317cbf59-en

InsightAce Analytic Pvt. (2023) Solid oxide electrolysis cell (SOEC) market. https://www.insightaceanalytic.com/report/solid-oxide-electrolysis-cell-soec-market/2076

IRENA (2019) Future of solar photovoltaic: Deployment, investment, technology, grid integration and socio-economic aspects. International Renewable Energy Agency, Abu Dhabi. https://www.irena.org/publications/2019/Nov/Future-of-Solar-Photovoltaic

IRENA (2020) Green hydrogen cost reduction: Scaling up electrolysers. International Renewable Energy Agency, Abu Dhabi. https://www.irena.org/-/media/Files/IRENA/Agency/Publication/2020/Dec/IRENA_Green_hydrogen_cost_2020.pdf

IRENA (2025) Renewable power generation costs in 2024. International Renewable Energy Agency, Abu Dhabi.

Kim J, Yoo D, Oh CH (2010) Simple electrolyser model development for high-temperature electrolysis system analysis using solid oxide electrolysis cell. J Nucl Sci Technol 47:599–607. https://doi.org/10.1080/18811248.2010.9720957

Jang D, Kim J, Han WH, Kang S (2022) Techno-economic analysis and Monte Carlo simulation of green hydrogen production technology through various water electrolysis technologies. Energy Convers Manag 258:115499. https://doi.org/10.1016/j.enconman.2022.115499

Jannati J, Nazarpour D (2017) Optimal energy management of the smart parking lot under demand response program in the presence of the electrolyser and fuel cell as hydrogen storage system. Energy Convers Manag 138:659–669. https://doi.org/10.1016/j.enconman.2017.02.030

Jiménez-Martín G, Judez X, Aguado M, Garbayo I (2024) Techno-economic assessment of MW-scale solid oxide electrolysis hydrogen production plant: Integrating possibilities in Spain. Int J Hydrogen Energy. https://doi.org/10.1016/j.ijhydene.2024.12.239

Jiménez-Martín G, Bąkała M, Judez X, Aguado M, Niemczyk A, Garbayo I (2025) Techno-economic feasibility of solid oxide electrolysis hybridization with solar photovoltaics and batteries for green hydrogen production. Energy Convers Manag X 27:101131. https://doi.org/10.1016/j.ecmx.2025.101131

Kalinci Y, Hepbasli A, Dincer I (2015) Techno-economic analysis of a stand-alone hybrid renewable energy system with hydrogen production and storage options. Int J Hydrogen Energy 40:7652–7664.

Khan MA, Al-Shankiti I, Ziani A, Idriss H (2021a) Demonstration of green hydrogen production using solar energy at 28% efficiency and evaluation of its economic viability. Sustain Energy Fuels 5:1085–1095. https://doi.org/10.1039/D0SE01761B

Khan MA, Young C, MacKinnon C, Layzell D (2021b) The techno-economics of hydrogen compression. Transition Accel Tech Briefs 1:1–36. ISSN 2564-1379.

Klymyshyn N, Brooks K, Barrett N (2023) Methods for estimating hydrogen fuel tank characteristics. J Press Vessel Technol Trans ASME 146. https://doi.org/10.1115/1.4063884

Kumar SS, Himabindu V (2019) Hydrogen production by PEM water electrolysis: A review. Mater Sci Energy Technol 2:442–454. https://doi.org/10.1016/j.mset.2019.03.002

Laguna-Bercero MA, Wang Y, Zhou XD, Zhu L (2023) Fundamentals of solid oxide electrolysis cells (SOEC). In: Laguna-Bercero MA (ed) High temperature electrolysis. Lect Notes Energy 95. Springer, Cham. https://doi.org/10.1007/978-3-031-22508-6_2

Lähdemäki E (2021) Process modelling and techno-economic analysis of solid oxide electrolyser system. Master thesis, School of Energy Systems, Energy Technology, LUT University. https://urn.fi/URN:NBN:fi-fe2021120859658

960 Lahrichi A, Issmaeli YE, et al. (2024) Advancements, strategies, and prospects of solid oxide electrolysis cells
961 (SOECs): Towards enhanced performance and large-scale sustainable hydrogen production.
962 https://doi.org/10.1016/j.jechem.2024.03.020

963 León-Vargas F, García-Jaramillo M, Krejci E (2019) Pre-feasibility of wind and solar systems for residential self-
964 sufficiency in four urban locations of Colombia: Implication of new incentives included in Law 1715. Renew Energy
965 130:1082–1091. https://doi.org/10.1016/j.renene.2018.06.087

966 León M, Silva J, Ortiz-Soto R, Carrasco S (2023) A techno-economic study for off-grid green hydrogen production
967 plants: The case of Chile. Energies 16:5327. https://doi.org/10.3390/en16145327

968 López AR, Krumm A, Schattenhofer L, Burandt T, Montoya FC, Oberländer N, Oei PY (2020) Solar PV generation
969 in Colombia: A qualitative and quantitative approach to analyze the potential of solar energy market. Renew Energy
970 148:1266–1279. https://doi.org/10.1016/j.renene.2019.10.066

971 Ley 1715 (2014) Por medio de la cual se regula la integración de las energías renovables no convencionales al Sistema
972 Energético Nacional. Congreso de la República de Colombia.
973 https://www.funcionpublica.gov.co/eva/gestornormativo/norma.php?i=57353

974 Ley 2099 (2021) Por medio de la cual se dictan disposiciones para la transición energética, la dinamización del
975 mercado energético, la reactivación económica del país y se dictan otras disposiciones. Congreso de la República de
976 Colombia. https://www.funcionpublica.gov.co/eva/gestornormativo/norma.php?i=166326

977 Maggio G, Squadrito G, Nicita A (2022) Hydrogen and medical oxygen by renewable energy based electrolysis: A
978 green and economically viable route. Appl Energy 306:117993. https://doi.org/10.1016/j.apenergy.2021.117993

979 Manuel C, Ortiz J, Rodriguez A (2023) A diffuse analysis based on analytical processes to prioritize barriers in the
980 development of renewable energy technologies in alignment with the United Nations Sustainable Development Goals:
981 Evidence from Guajira/Colombia. Int J Energy Econ Policy 13:481–195. https://doi.org/10.32479/ijeep.14380

982 Martínez-González OE, Morales-Medina G, Quiroga-Becerra H (2024) Analysis of the operation of an industrial
983 reforming furnace based on plant data and process simulation. CT&F Cienc Tecnol Futuro 14:13–28.
984 https://doi.org/10.29047/01225383.751

Martsinchyk K, Martsinchyk A, Łazor M, Shuhayeu P, Kupecki J, Niemczyk A, Błesznowski M, Milewski J (2024) Feasibility study and techno-economic assessment of power-to-gas (P2G) technology based on solid oxide electrolysis (SOE). J Environ Manag 354:120425. https://doi.org/10.1016/j.jenvman.2024.120425

Masters GM (2013) Renewable and efficient electric power systems. 2nd ed. John Wiley & Sons, Hoboken, NJ.

Mauler L, Duffner F, Zeier WG, Leker J (2021) Battery cost forecasting: A review of methods and results with an outlook to 2050. Energy Environ Sci 14:4712–4739. https://doi.org/10.1039/d1ee01530c

McCormick BA, Harrison SJ, Pharoah JG (2016) An annual model of a solar-hydrogen energy storage system. eSim 2016 Conference Proceedings: 9th Conference of IBPSA-Canada, Hamilton, May 4–5. http://www.ibpsa.org/proceedings/eSimPapers/2016/42-156-eSim2016.pdf

McKellar MG, O'Brien JE, Harvego EA, Herring JS (2007) Optimized flow-sheet for a reference commercial-scale nuclear-driven high temperature electrolysis hydrogen production plant. Idaho National Laboratory Report No. INL/EXT-07-13573. https://doi.org/10.2172/924513

Minenergía (2021) Hoja de Ruta del Hidrógeno en Colombia. https://www.minenergia.gov.co/es/micrositios/enlace-ruta-hidrogeno/

Ministerio de la Protección Social (2009) Resolución 4410 de 2009. Reglamento Técnico que contiene el Manual de Buenas Prácticas de Manufactura de los Gases Medicinales. https://www.suin-juriscol.gov.co/viewDocument.asp?ruta=Resolucion/30033898

Monforti-Ferrario A, Bartolini A, Segura-Manzano F, Vivas FJ, Comodi G, McPhail SJ, Andujar JM (2021) A model-based parametric and optimal sizing of a battery/hydrogen storage of a real hybrid microgrid supplying a residential load: Towards island operation. Adv Appl Energy 3:100048. https://doi.org/10.1016/j.adapen.2021.100048

Moreno J, Cobo M, Barraza-Botet C, Sanchez N (2022) Role of low carbon emission H2 in the energy transition of Colombia: Environmental assessment of H2 production pathways for a certification scheme. Energy Convers Manag X 16:100312. https://doi.org/10.1016/j.ecmx.2022.100312

Motazedi K, Salkuyeh YK, Laurenzi IJ, MacLean HL, Bergerson JA (2021) Economic and environmental competitiveness of high temperature electrolysis for hydrogen production. Int J Hydrogen Energy 46:21274–21288. https://doi.org/10.1016/j.ijhydene.2021.03.226

Mulcué-Nieto LF (2020) Desarrollo de nuevos modelos para la fotovoltaica integrada en edificios (BIPV) en ciudades sostenibles. Tesis doctoral, Escuela de Ingenierías Industriales, Universidad de Málaga. https://hdl.handle.net/10630/19809

Muñoz Y, Suarez CA, Castro AO, López OJ (2024) Technical and financial analysis for the implementation of small-scale self-generation projects, based on grid-tied photovoltaic solar energy, for residential users under Colombian regulations. Int J Energy Econ Policy 14:197–205. https://doi.org/10.32479/ijeep.14958

Nadaleti WC, de Souza EG, Lourenço VA (2022) Green hydrogen-based pathways and alternatives: Towards the renewable energy transition in South America's regions–Part B. Int J Hydrogen Energy 47:1–15. https://doi.org/10.1016/j.ijhydene.2021.05.113

Naeini M, Cotton J, Adams TA (2022) An eco-technoeconomic analysis of hydrogen production using solid oxide electrolysis cells that accounts for long-term degradation. Front Energy Res 10. https://doi.org/10.3389/fenrg.2022.1015465

Ni M, Leung MKH, Leung DYC (2007) Energy and exergy analysis of hydrogen production by solid oxide steam electrolyzer plant. Int J Hydrogen Energy 32:4648–4660. https://doi.org/10.1016/j.ijhydene.2007.08.005

NREL (2023) Annual Technology Baseline. https://atb.nrel.gov/electricity/2023/definitions#inflation

O'Brien JE, Stoots CM, Herring JS, Hawkes GL (2005) Comparison of a one-dimensional model of a high-temperature solid-oxide electrolysis stack with CFD and experimental results. ASME IMECE:117–126.

O'Hayre R, Cha SW, Colella WG (2009) Fuel cell fundamentals. 2nd ed. John Wiley & Sons, Hoboken, NJ.

Paneru B, Paudel A, Paneru B, Alexander V, Mainali DP, Karki S, Karki S, Thapa SB, Poudyal KN, Poudyal R (2024) Techno-economic analysis of green hydrogen production, storage, and waste heat recovery plant in the context of Nepal. Int J Hydrogen Energy 77:892–905. https://doi.org/10.1016/j.ijhydene.2024.06.161

Perez A, Garcia-Rendon JJ (2020) Integration of non-conventional renewable energy and spot price of electricity: A counterfactual analysis for Colombia. Renew Energy. https://doi.org/10.1016/j.renene.2020.11.067

Perna A, Minutillo M, Di Micco S, Jannelli E (2022) Design and costs analysis of hydrogen refuelling stations based on different hydrogen sources and plant configurations. Energies 15:541. https://doi.org/10.3390/en15020541

Peters MS, Timmerhaus KD, West RE (2002) Plant design and economics for chemical engineers. 5th ed. McGraw-Hill Professional.

Plazas-Niño F, Yeganyan R, Cannone C, Howells M, Borba B, Quirós-Tortós J (2023) The role of low-emission hydrogen in developing countries: A techno-economic assessment of hydrogen pathways in Colombia. Cambridge Open Engage. https://doi.org/10.33774/coe-2023-vr3hr. Preprint, not peer-reviewed.

Portafolio (2024) EPM logró la producción de hidrógeno verde con biogás de aguas residuales. https://www.portafolio.co/energia/epm-logro-la-produccion-de-hidrogeno-verde-con-biogas-de-aguas-residuales-599410

Posdziech O, Geißler T, Schwarze K, Blumentritt R (2019) System development and demonstration of large-scale high-temperature electrolysis. ECS Trans 91:2537–2546. https://doi.org/10.1149/09101.2537ecst

Promigas (2022) Hidrógeno: El combustible del futuro descarbonizado. https://www.promigas.com/InformeSectorGas2022/Paginas/Hidrogeno.aspx

Prosser JH, James BD, Murphy BM, Wendt D, Casteel M, Westover TL, Knighton LT (2023) Cost analysis of hydrogen production by high-temperature solid oxide electrolysis. Int J Hydrogen Energy. https://doi.org/10.1016/j.ijhydene.2023.07.084

Ramasamy V, Woodhouse M, Feldman D (2025) Q1-2025 solar photovoltaic system cost benchmarks. United States. https://doi.org/10.7799/3009689

Ranjbar F, Chitsaz A, Mahmoudi SMS, Khalilarya S, Rosen MA (2014) Energy and exergy assessments of a novel trigeneration system based on a solid oxide fuel cell. Energy Convers Manag 87:318–327. https://doi.org/10.1016/j.enconman.2014.07.014

Reddi K, Elgowainy A, Rustagi N, Gupta E (2018) Techno-economic analysis of conventional and advanced high-pressure tube trailer configurations for compressed hydrogen gas transportation and refueling. Int J Hydrogen Energy 43:4428–4438. https://doi.org/10.1016/j.ijhydene.2018.01.049

Rincón-Montenegro A, Carmona M, Sanjuan M, Ramirez A, Portnoy I (2024) Multi-criteria assessment of transition scenarios for a novel hybrid power and hydrogen generation system. Energy Convers Manag 313:118552. https://doi.org/10.1016/j.enconman.2024.118552

Rodríguez-Fontalvo D, Quiroga E, Cantillo NM, Sánchez N, Figueredo M, Cobo M (2023) Green hydrogen potential in tropical countries: The Colombian case. Int J Hydrogen Energy 54:344–360. https://doi.org/10.1016/j.ijhydene.2023.03.320

Ropero-Castaño W, Muñoz-Galeano N, Caicedo-Bravo EF, Maya-Duque P, López-Lezama JM (2022) Sizing assessment of islanded microgrids considering total investment cost and tax benefits in Colombia. Energies 15:5161. https://doi.org/10.3390/en15145161

Sadeghi M, Chitsaz A, Mahmoudi SMS, Rosen MA (2015) Thermoeconomic optimization using an evolutionary algorithm of a trigeneration system driven by a solid oxide fuel cell. Energy 89:191–204. https://doi.org/10.1016/j.energy.2015.07.067

Sadiq M, Alshehhi RJ, Urs RR, Mayyas AT (2023) Techno-economic analysis of Green-H2@Scale production. Renew Energy 219:119362. https://doi.org/10.1016/j.renene.2023.119362

Sakas G, Ibáñez-Rioja A, Ruuskanen V, Kosonen A, Ahola J, Bergmann O (2022) Dynamic energy and mass balance model for an industrial alkaline water electrolyser plant process. Int J Hydrogen Energy 47:4328–4345. https://doi.org/10.1016/j.ijhydene.2021.11.126

Sallyth A, Ramos V (2021) Economic viability and optimization of solar microgrids with hybrid storage in a non-interconnected zone in Colombia. Environ Dev Sustain 23:12842–12866. https://doi.org/10.1007/s10668-020-01188-w

Sánchez-Squella A, Muñoz M, Toledo M, Yanine F (2025) Techno-economic assessment of a green hydrogen production plant for a mining operation in Chile. Int J Hydrogen Energy 112:531–543. https://doi.org/10.1016/j.ijhydene.2025.02.164

Schmidt O, Gambhir A, Staffell I, Hawkes A, Nelson J, Few S (2017) Future cost and performance of water electrolysis: An expert elicitation study. Int J Hydrogen Energy 42:30470–30492. https://doi.org/10.1016/j.ijhydene.2017.10.045

Seider WD, Lewin DR, Seader JD, Widagdo S, Gani R, Ming-Ng K (2017) Product and process design principles: Synthesis, analysis and evaluation. 4th ed. Wiley.

Semana (2022a) Ecopetrol invirtió US$6 millones para poner en marcha su piloto de hidrógeno verde. https://www.semana.com/economia/empresas/articulo/ecopetrol-invirtio-us-6-millones-para-poner-en-marcha-su-piloto-de-hidrogeno-verde/202232/

Semana (2022b) Promigas comienza su apuesta por el hidrógeno verde con proyecto piloto en Cartagena. https://www.semana.com/economia/empresas/articulo/promigas-comienza-su-apuesta-por-el-hidrogeno-verde-con-proyecto-piloto-en-cartagena/202211/

Shehabi M, Dally B (2021) Opportunity and cost of green hydrogen production in Kuwait: A preliminary assessment. USAEE Working Paper No. 21-536. https://ssrn.com/abstract=3995610; https://doi.org/10.2139/ssrn.3995610

Sladkovskiy DA, Godina LI, Semikin KV, Sladkovskaya EV, Smirnova DA, Murzin DY (2018) Process design and techno-economical analysis of hydrogen production by aqueous phase reforming of sorbitol. Chem Eng Res Des 134:104–116. https://doi.org/10.1016/j.cherd.2018.03.041

Stangarone T (2021) South Korean efforts to transition to a hydrogen economy. Clean Techn Environ Policy 23:509–516. https://doi.org/10.1007/s10098-020-01936-6

Sun H, Ikram M, Mohsin M, Abbas Q (2021) Energy security and environmental efficiency: Evidence from OECD countries. Singap Econ Rev 66:489–506.

Tomberg M (2024) Experimental operation, modelling and simulation of solid oxide cell reactors with multiple stacks for process systems. Doctoral dissertation, Universität Stuttgart.

Trinke P, Bensmann B (2017) Current density effect on hydrogen permeation in PEM water electrolysers. Int J Hydrogen Energy 42:14355–14366. https://doi.org/10.1016/j.ijhydene.2017.03.231

US Department of Energy (2020) Hydrogen Program Plan. https://www.hydrogen.energy.gov/library/roadmaps-vision

Utgikar V, Thiesen T (2006) Life cycle assessment of high temperature electrolysis for hydrogen production via nuclear energy. Int J Hydrogen Energy 31:939–944. https://doi.org/10.1016/j.ijhydene.2005.07.001

Vargas-Reyes LS, González-Martínez AC, Morales-Medina G (2023) Variations in associated gas CO_2 concentration: Evaluation of the performance of a turboexpander gas conditioning unit. Rev Fuentes El Reventón Energ 21:103–119. https://doi.org/10.18273/revfue.v21n2-2023007

Vartiainen E, Breyer C, Moser D, Román Medina E, Busto C, Masson G, Bosch E, Jäger-Waldau A (2021) True cost of solar hydrogen. Solar RRL:2100487. https://doi.org/10.1002/solr.202100487

Velasquez-Jaramillo M, García JG, Vasco-Echeverri O (2024) Techno economic model to analyze the prospects of hydrogen production in Colombia. Int J Thermofluids 22:100597. https://doi.org/10.1016/j.ijft.2024.100597

Vidas L, Castro R (2021) Recent developments on hydrogen production technologies: State-of-the-art review with a focus on green-electrolysis. Appl Sci 11:11363. https://doi.org/10.3390/app112311363

Vives AMV, Wang R, Roy S, Smallbone A (2023) Techno-economic analysis of large-scale green hydrogen production and storage. Appl Energy 346:121333. https://doi.org/10.1016/j.apenergy.2023.121333

Walas SM (1988) Chemical process equipment: Selection and design. Butterworth-Heinemann.

Wang F, Wang L, Ou Y, Lei X, Yuan J, Liu X, Zhu Y (2021) Thermodynamic analysis of solid oxide electrolyser integration with engine waste heat recovery for hydrogen production. Case Stud Therm Eng 27:101240. https://doi.org/10.1016/j.csite.2021.101240

Wang L, Chen M, Küngas R, Lin TE, Diethelm S, Maréchal F, Van Herle J (2019) Power-to-fuels via solid-oxide electrolyser: Operating window and techno-economics. Renew Sustain Energy Rev 110:174–187. https://doi.org/10.1016/j.rser.2019.04.071

Yan P, Li K (2025) Design and operational considerations of micro-structured solid oxide electrolysis cells for sustainable and economic hydrogen production. Int J Hydrogen Energy 157:150417. https://doi.org/10.1016/j.ijhydene.2025.150417

Zainal BS, Ker PJ, Mohamed H, Ong HC, Fattah IMR, Rahman S, Nghiem LD, Mahlia TMI (2024) Recent advancement and assessment of green hydrogen production technologies. Renew Sustain Energy Rev 189:113941. https://doi.org/10.1016/j.rser.2023.113941

Zghaibeh M, Barhoumi EM, Okonkwo PC, Belgacem IB, Beitelmal WH, Mansir IM (2022) Analytical model for a techno-economic assessment of green hydrogen production in photovoltaic power station case study Salalah city-Oman. Int J Hydrogen Energy 47:14171–14179. https://doi.org/10.1016/j.ijhydene.2022.02.180

Zhang L, Ma F, Zeng Q, Peng F, Hu Q, Wu K, Yang Y, Lu H, Liang B (2022) Direct methanation of CO_2 in biogas with hydrogen from water electrolysis: The catalyst and system efficiency. Energy Fuels 36:4416–4426. https://doi.org/10.1021/acs.energyfuels.2c00437

Zhao Y, Xue H, Jin X, Xiong B, Liu R, Peng Y, Jiang L, Tian G (2021) System level heat integration and efficiency analysis of hydrogen production process based on solid oxide electrolysis cells. Int J Hydrogen Energy 46:38163–38174. https://doi.org/10.1016/j.ijhydene.2021.09.105

Zoulias EI, Lymberopoulos N (2007) Techno-economic analysis of the integration of hydrogen energy technologies in renewable energy-based stand-alone power systems. Renew Energy 32:680–696. https://doi.org/10.1016/j.renene.2006.02.005

Supplementary Files

This is a list of supplementary files associated with this preprint. Click to download.

- Suplementarymaterial.docx